AD_____

Award Number: DAMD17-02-1-0119

TITLE: Sodium Iodide Symporter Gene Transfer for Imaging and Ablation of Prostate Cancer

PRINCIPAL INVESTIGATOR: Sissy M. Jhiang, Ph.D.

CONTRACTING ORGANIZATION: The Ohio State University Research Foundation
Columbus, Ohio 43210-1063

REPORT DATE: January 2004

TYPE OF REPORT: Annual

PREPARED FOR: U.S. Army Medical Research and Materiel Command
Fort Detrick, Maryland 21702-5012

REPORT DOCUMENTATION PAGE

Form Approved
OMB No. 074-0188

1. AGENCY USE ONLY (Leave blank)	2. REPORT DATE	3. REPORT TYPE AND DATES COVERED
	January 2004	Annual (15 Dec 2002 - 14 Dec 2003)

4. TITLE AND SUBTITLE
Sodium Iodide Symporter Gene Transfer for Imaging and Ablation of Prostate Cancer

5. FUNDING NUMBERS
DAMD17-02-1-0119

6. AUTHOR(S)
Sissy M. Jhiang, Ph.D.

7. PERFORMING ORGANIZATION NAME(S) AND ADDRESS(ES)
The Ohio State University Research Foundation
Columbus, Ohio 43210-1063

E-Mail: jhiang.1@osu.edu

8. PERFORMING ORGANIZATION REPORT NUMBER

9. SPONSORING / MONITORING AGENCY NAME(S) AND ADDRESS(ES)
U.S. Army Medical Research and Materiel Command
Fort Detrick, Maryland 21702-5012

10. SPONSORING / MONITORING AGENCY REPORT NUMBER

11. SUPPLEMENTARY NOTES
Original contains color plates: All DTIC reproductions will be in black and white.

12a. DISTRIBUTION / AVAILABILITY STATEMENT
Approved for Public Release; Distribution Unlimited

12b. DISTRIBUTION CODE

13. ABSTRACT (Maximum 200 Words)
The sodium iodide symporter (NIS) mediates iodide uptake in thyroid follicular cells and provides a mechanism for effective radioiodide treatment of residual, recurrent, and metastatic thyroid cancers. The objective of the proposed research is to test the hypothesis that expression of exogenous hNIS in prostatic tissue will enable radioiodide to localize and ablate residual prostate cancer following prostatectomy, such that recurrence and metastasis of the disease can be prevented. The specific aims of this project are to: (1) confirm metastatic progression to distant lymph nodes and lungs following subcutaneous inoculation of rats with MATLyLu prostatic adenocarcinoma cells expressing hNIS; (2) investigate whether radioiodide therapy will prevent metastases and/or prolong survival in rats bearing subcutaneous MATLyLu tumors that express hNIS; (3) determine the expression level of hNIS required to elicit selective radioiodide-mediated killing of MATLyLu-hNIS prostatic adeoncarcinoma cells in vivo; and, (4) restrict hNIS expression in prostatic tissue under transcriptional regulation of prostate-specific promoter.

14. SUBJECT TERMS
Prostate cancer, sodium iodide symporter, gene transfer, radioiodide

15. NUMBER OF PAGES
31

16. PRICE CODE

17. SECURITY CLASSIFICATION OF REPORT	18. SECURITY CLASSIFICATION OF THIS PAGE	19. SECURITY CLASSIFICATION OF ABSTRACT	20. LIMITATION OF ABSTRACT
Unclassified	Unclassified	Unclassified	Unlimited

Table of Contents

INTRODUCTION

The sodium iodide symporter (NIS) mediates iodide uptake in thyroid follicular cells and provides a mechanism for effective radioiodide treatment of residual, recurrent, and metastatic thyroid cancers. The objective of the proposed research is to test the hypothesis that expression of exogenous hNIS in prostatic tissue will enable radioiodide to localize and ablate residual prostate cancer following prostatectomy, such that recurrence and metastasis of the disease can be prevented. The specific aims of this project are to: (1) confirm metastatic progression to distant lymph nodes and lungs following subcutaneous inoculation of rats with MATLyLu prostatic adenocarcinoma cells expressing hNIS; (2) investigate whether radioiodide therapy will prevent metastases and/or prolong survival in rats bearing subcutaneous MATLyLu tumors that express hNIS; (3) determine the expression level of hNIS required to elicit selective radioiodide-mediated killing of MATLyLu-hNIS prostatic adenocarcinoma cells *in vivo*; and, (4) restrict hNIS expression in prostatic tissue under transcriptional regulation of prostate-specific promoter.

BODY

Task 1. Confirm metastatic progression to distant lymph nodes and lungs following subcutaneous inoculation of rats with MATLyLu prostatic adenocarcinoma cells expressing hNIS: ***Completed in Year 1 with one published paper***

KMD La Perle, D Shen, TLF Buckwalter, B Williams, A Haynam, G Hinkle, R Pozderac, CC Capen, and SM **Jhiang** (2002) "*In Vivo* Expression and Function of the Sodium Iodide Symporter Following Gene Transfer in the MATLyLu Rat Model of Metastatic Prostate Cancer", *The Prostate*, **50**: 170-178.

Task 2. Investigate whether radioiodide therapy will prevent metastases and/or prolong survival in rats bearing subcutaneous MATLyLu tumors that express hNIS (Months 12-24, ***completed***)

***Appendix 1*:** KMD La Perle, EAG Blomme, CC Capen, and SM **Jhiang** (2003) "Effect of Exogenous Human Sodium/Iodide Symporter Expression on Growth of MatLyLu Cells", *Thyroid* **13:**133-140

***Appendix 2*:** DHY Shen, DK Marsee, J Schaap, W Yang, J-Y Cho, G Hinkle, HN Nagaraja, RT Kloos, RF Barth, and SM **Jhiang** (2004) "Effects of dose, intervention time, and radionuclide on sodium iodide symporter (NIS) targeted radionuclide therapy", *Gene Therapy* **11:** 161-169.

As reported in the previous annual report, we found that NIS expression inhibits MATLyLu cell growth (La Perle et al, 2003). We also found that the time course of tumor progression and spread of metastases vary significantly among animals even in the same experimental group (La Perle et al, 2002, and La Perle et al, 2003). Thus, we have chosen an alternative animal model to investigate the therapeutic effectiveness of NIS-

mediated radioiodide therapy (Shen et al, 2004). The effectiveness of NIS as a gene therapy agent lies in its ability to mediate the uptake of a variety of radionuclides, such as ^{131}I, ^{125}I, and $^{188}ReO_4$. We have conducted a study comparing the therapeutic effectiveness of these different radionuclides in NIS-expressing gliomas, which have relatively uniform survival time among untreated animals. We show that: (1) the therapeutic effectiveness of ^{131}I in prolonging the survival time of rats bearing F98/hNIS gliomas is dose- and treatment-time-dependent; (2) the number of remaining NIS expressing tumor cells decreased greatly in RG2/hNIS gliomas post ^{131}I treatment and was inversely related to survival time; (3) 8 mCi each of $^{125}I/^{131}I$ is as effective as 16 mCi ^{131}I alone, despite a smaller tumor absorbed dose; (4) $^{188}ReO_4$, a potent $\tilde{\beta}$ emitter, is more efficient than ^{131}I to enhance the survival of rats bearing F98/hNIS gliomas. These studies demonstrate the importance of radiopharmaceutical selection, dose, and timing of treatment to optimize the therapeutic effectiveness of NIS-targeted radionuclide therapy.

Task 3. Determine the expression level of hNIS required to elicit selective radioiodide-mediated killing of MatLyLu-hNIS prostatic adenocarcinoma cells *in vivo* (months 18-36, in progress)

We hypothesize that radioiodide uptake *in vivo* correlates with NIS expression levels within a certain range. We have been trying to establish MatLyLu clonal cells with doxycycline-inducible NIS expression so that we could determine the range of NIS expression levels required to elicit radioiodide-mediated killing effects. Unfortunately, we have failed to acquire doxycycline-inducible MatLyLu-hNIS clones despite several attempts. However, we have been able to establish doxycycline-inducible hNIS clones using other cell lines. We are now trying to switch to other human prostate cancer cell lines to accomplish this task.

Task 4. Restrict hNIS expression in prostatic tissue under transcriptional regulation of prostate-specific promoters (Months 1-36, in progress)

Appendix 3: DK Marsee, DHY Shen, LR MacDonald, DD Vadysirisack, X Lin, G Hinkle, RT Kloos, SM Jhiang (2004) "Imaging of Pulmonary Tumors Following NIS Gene Transfer Using Single Photon Emission Computed Tomography", *Cancer Gene Therapy* in press.

Since the most challenging issues of gene therapy remains vector delivery to the target tissue, we have been trying to use NIS as imaging reporter gene to optimize vector delivery efficiency, in addition to engineer adenovirus carrying NIS under the control of prostate-specific promoter. Due to the high mortality associated with pulmonary tumor metastases, we have focused our MatLyLu studies on the use of NIS in gene therapy for lung tumor nodules (Marsee et al, 2004). In this study, we established NIS-expressing pulmonary tumors in nude mice by intravenous injection of tumor cells and investigated the minimal tumor size required for *in vivo* detection of pulmonary tumors by single photon emission computed tomography (SPECT) with pinhole collimation. In order to define the anatomic location of NIS-expressing tumor nodules detectable by SPECT, we performed simultaneous, dual-isotope imaging. We injected 1 mCi ^{99m}Tc-

MAA via tail vein to image pulmonary perfusion and injected 1 mCi $Na^{125}I$ intraperitoneally to image NIS-expressing tumors. Fused images showed that ^{99m}Tc-MAA perfusion defects correlated with NIS-mediated ^{125}I uptake. Post-mortem analysis revealed that tumors 3 mm in diameter could be detected by SPECT with pinhole collimation. These studies demonstrate the feasibility of SPECT to detect pulmonary tumors expressing exogenous NIS in mice.

We have also been exploring different methods to efficiently deliver adenoviruses to MatLyLu pulmonary tumor nodules. *In vitro* studies demonstrated that MatLyLu cells are highly susceptible to adenoviral infection. Initially, we attempted to deliver adenoviruses via intravenous delivery. Viral gene expression was found in the liver, but not in either the lung parenchyma or pulmonary tumor nodules. We also performed intratracheal injection to deliver viruses to pulmonary tumors. Whereas the lung parenchyma showed strong viral gene expression, the tumor nodules were not infected. These results suggest that MatLyLu pulmonary tumors do not communicate with the alveolar airspace, likely due to the localization of MatLyLu tumors on the surface of the lung. We are currently in the process of performing intrapleural adenoviral delivery as a means to infect pulmonary metastases.

KEY RESEARCH ACCOMPLISHMENTS

- Demonstrate the importance of radiopharmaceutical selection, dose, and timing of treatment to optimize the therapeutic effectiveness of NIS-targeted radionuclide therapy
- Demonstrate the feasibility of single photon emission computed tomography (SPECT) to non-invasively detect pulmonary metastases of MatLyLu-hNIS tumors with a diameter of 3 mm in size in mice.

REPORTABLE OUTCOMES

Manuscript 1: KMD La Perle, EAG Blomme, CC Capen, and SM **Jhiang** (2003) "Effect of Exogenous Human Sodium/Iodide Symporter Expression on Growth of MatLyLu Cells", *Thyroid* **13:**133-140

Manuscript 2: DHY Shen, DK Marsee, J Schaap, W Yang, J-Y Cho, G Hinkle, HN Nagaraja, RT Kloos, RF Barth, and SM **Jhiang** (2004) "Effects of dose, intervention time, and radionuclide on sodium iodide symporter (NIS) targeted radionuclide therapy", *Gene Therapy* **11:** 161-169.

Manuscript 3: DK Marsee, DHY Shen, LR MacDonald, DD Vadysirisack, X Lin, G Hinkle, RT Kloos, SM Jhiang (2004) "Imaging of Pulmonary Tumors Following NIS Gene Transfer Using Single Photon Emission Computed Tomography", *Cancer Gene Therapy* in press.

CONCLUSIONS

- Selecting the optimal radiopharmaceuticals, as well as the optimal dose and timing of treatment, could further optimize NIS-targeted radionuclide therapy for prostate cancer.

- NIS can serve as an imaging reporter gene to optimize vector delivery for prostate cancer gene therapy.

REFERENCES

KMD La Perle, D Shen, TLF Buckwalter, B Williams, A Haynam, G Hinkle, R Pozderac, CC Capen, and SM **Jhiang** (2002) "*In Vivo* Expression and Function of the Sodium Iodide Symporter Following Gene Transfer in the MATLyLu Rat Model of Metastatic Prostate Cancer", *The Prostate*, **50**: 170-178.

KMD La Perle, EAG Blomme, CC Capen, and SM **Jhiang** (2003) "Effect of Exogenous Human Sodium/Iodide Symporter Expression on Growth of MatLyLu Cells", *Thyroid* **13:**133-140

DHY Shen, DK Marsee, J Schaap, W Yang, J-Y Cho, G Hinkle, HN Nagaraja, RT Kloos, RF Barth, and SM **Jhiang** (2004) "Effects of dose, intervention time, and radionuclide on sodium iodide symporter (NIS) targeted radionuclide therapy", *Gene Therapy* **11:** 161-169.

DK Marsee, DHY Shen, LR MacDonald, DD Vadysirisack, X Lin, G Hinkle, RT Kloos, SM Jhiang (2004) "Imaging of Pulmonary Tumors Following NIS Gene Transfer Using Single Photon Emission Computed Tomography", *Cancer Gene Therapy* in press.

APPENDICES

Three manuscripts are appended.

THYROID
Volume 13, Number 2, 2003

Appendix 1

Effect of Exogenous Human Sodium Iodide Symporter Expression on Growth of MATLyLu Cells

Krista M.D. La Perle,[1] Eric A.G. Blomme,[2] Charles C. Capen,[1] and Sissy M. Jhiang[1,3]

The sodium iodide symporter (NIS) mediates iodide uptake in thyroid cells and enables the effective radioiodide treatment of thyroid cancers. There is much interest in facilitating radioiodide therapy in other cancers by NIS gene transfer. This study showed that exogenous NIS expression decreased MATLyLu rat prostatic adenocarcinoma cell growth. Tumor growth and metastatic progression were significantly delayed in syngeneic rats injected with mixed or clonal populations of MATLyLu-NIS cells compared to rats with control tumors. MATLyLu-NIS tumors in nude mice had a lower, albeit not statistically significant, growth rate than control tumors. The Ki-67 labeling index in NIS-positive areas was lower than in NIS-negative areas of rat tumors derived from a mixed population of MATLyLu-NIS cells. Growth of clonal populations of MATLyLu-NIS cells was delayed *in vitro*. These results demonstrate that NIS expression inhibits MATLyLu cell growth, thereby providing an additional potential benefit of NIS-mediated gene therapy for cancer.

INTRODUCTION

THE INHERENT ABILITY of the thyroid gland to transport iodide is mediated by the sodium (Na^+)/iodide (I^-) symporter (NIS) (1). This 13-transmembrane glycoprotein present on the basolateral membrane of thyroid follicular epithelial cells couples the inward movement of two Na^+ ions with one I^- ion in an active process driven by a Na^+/K^+ adenosine triphosphatase (ATPase) (1). Consequently, the thyroidal intracellular concentration of I^- is 20- to 40-fold higher than that in plasma (1). This uptake of I^- is a crucial step in the production of the thyroid hormones, triiodothyronine (T_3) and tetraiodothyronine or thyroxine (T_4). In addition, this aspect of normal thyroid physiology has been successfully exploited for the localization and ablation of residual, recurrent, and metastatic thyroid cancer subsequent to radionuclide administration. The standard therapeutic regimen for thyroid cancer, which combines thyroidectomy followed by radioiodide therapy, has contributed to excellent 10-year survival rates and low recurrence and mortality rates with minimal side effects (2).

As a result of this success in treating thyroid cancer, gene therapy strategies using NIS have become attractive for the treatment of various types of cancer. In recent years, several studies have investigated the clinical applications of either rat (rNIS) or human (hNIS) NIS gene transfer by nonviral and viral methods for *in vitro* cell killing, *in vivo* imaging, and/or radioiodide therapy of cervical, breast, hepatic, thyroid, and prostate cancer, and melanoma xenografts in rodents (3–11). The majority of these studies have utilized immunodeficient mice bearing subcutaneous human cancer xenografts (3,4,6,8,10,11), with fewer studies using syngeneic rat models (5,7,9). We recently reported the detection of subcutaneous tumors and metastases in lymph nodes by nuclear scintigraphy following *ex vivo* retroviral gene transfer of hNIS in the MATLyLu syngeneic rat model of metastatic prostate cancer (9). During the course of this study, we observed that NIS-transduced tumors were smaller and progressed at a slower rate *in vivo* than parental or vector-transduced tumors. The aim of the current study was to explore this further and determine the effect of hNIS expression on the growth of MATLyLu rat prostatic adenocarcinoma cells *in vitro* and *in vivo* in the absence of radioiodide therapy.

Materials and Methods

Recombinant hNIS retrovirus

Recombinant retroviral DNA constructs containing either hNIS#9 cDNA or FLhNIS cDNA were engineered using the retroviral vector LXSN (kindly provided by Dr. Kathleen Boris-Lawrie, The Ohio State University, Columbus, OH) to produce L-hNIS-SN. The protein encoded by hNIS#9 is truncated because of the absence of the last 31 amino acids at the C-terminus. This truncated protein is functional; however, available anti-hNIS antibodies recognize the C-terminus of

[1]Department of Veterinary Biosciences, The Ohio State University, Columbus, Ohio.
[2]Pharmacia, Skokie, Illinois.
[3]Department of Physiology and Cell Biology, The Ohio State University, Columbus, Ohio.

the FLhNIS. L-hNIS-SN expresses hNIS cDNA under the control of the 5′ Moloney murine leukemia virus long terminal repeat promoter (L) and expresses a neomycin resistance gene (N) under the control of an internal simian virus 40 promoter (S) (12). Retrovirus was generated as previously described (9).

MATLyLu cells and syngeneic Copenhagen rat animal model

The MATLyLu cell line is one of several sublines developed from a spontaneous prostatic adenocarcinoma in a Copenhagen rat (13). The MATLyLu subline is a rapidly growing, androgen-independent, anaplastic cell line that is highly metastatic to ipsilateral lymph nodes and lungs after subcutaneous injection in syngeneic Copenhagen rats (14–16). MATLyLu cells were obtained from Dr. Laurie K. McCauley (Department of Periodontics/Prevention/Geriatrics, University of Michigan, Ann Arbor, MI), the European Collection of Cell Cultures (ECACC, #94101454, Salisbury, Wiltshire, United Kingdom), and Dr. Albert A. Geldof (Academisch Ziekenhuis Vrije Universiteit, Amsterdam, The Netherlands), and were maintained in RPMI-1640 supplemented with 10% fetal bovine serum, 100 U/mL of penicillin G sodium, 100 μg/mL of streptomycin sulfate, 2 mM of L-glutamine, 1 mM of sodium pyruvate, 10 mg/mL of insulin, 5.5 mg/mL of transferrin, and 6.7 μg/mL or sodium selenite. All cell culture media and reagents were purchased from Gibco-BRL Life Technologies, Inc. (Grand Island, NY) unless otherwise stated. Cells were transduced by incubation with 1 mL of filtered L-hNIS#9-SN, L-FLhNIS-SN, or LXSN retrovirus in maintenance media for 24 hours. Selection of transduced MATLyLu cells was performed with 800 μg/mL Geneticin (G418) for 5 days followed by maintenance in 400 μg/mL G418. Individual clones, as well as mixed populations of transduced MATLyLu cells were expanded and used for *in vitro* and *in vivo* studies. NIS expression in transduced cells was confirmed *in vitro* by iodide uptake assays as previously reported (9). Two- to 3-month-old male Copenhagen rats (Harlan-Sprague Dawley, Indianapolis, IN) were subcutaneously injected using a 26-gauge needle in the right flank with 1×10^6 cells suspended in 0.5 mL of Hanks balanced salt solution (HBSS). Rats were allowed *ad libitum* access to water and standard rodent chow. All experimental procedures in this study received approval from the Institutional Laboratory Animal Care and Use Committee of The Ohio State University. Tumor size at the site of injection was measured with microcalipers weekly and at necropsy, and tumor volumes were calculated in cubic centimeters using the equation: volume = length × width × height × 0.5236 (17).

Tumorigenicity in nude mice

One million cells were resuspended in 200 μL of phosphate-buffered saline and subcutaneously injected using a 26-gauge needle in the left (parental MATLyLu cells, $n = 6$; MATLyLu-LXSN-mixed, $n = 6$) and right (MATLyLu-FLhNIS-mixed, $n = 12$) flanks of BALB/c athymic nude mice (male, 6–8 weeks old; Harlan Sprague Dawley). Mice were maintained under pathogen-free conditions and allowed *ad libitum* access to water and standard rodent chow. Tumor size at the site of injection was measured with microcalipers three times per week and at necropsy, and tumor volumes were calculated in cubic millimeters as described above.

Histopathology

Complete postmortem and histopathologic evaluations were performed on all rodents. Portions of the subcutaneous tumors, lymph node metastases, and lungs were fixed in 10% neutral-buffered formalin, routinely processed and embedded in paraffin. Sections (5 μm) were stained with hematoxylin and eosin (H&E).

Immunohistochemistry

Immunohistochemical staining was performed on 5-μm paraffin sections cut onto poly-L-lysine slides. NIS immunohistochemistry was performed as previously described with a few modifications (18). Briefly, slides were incubated for 30 minutes in 10 mM citric acid buffer (pH 6.0) at 94°C for antigen retrieval. Endogenous peroxidase was inhibited by 3% hydrogen peroxide in methanol. Tissue sections were incubated with an anti-hNIS proprietary polyclonal rabbit antibody (#331; 1:250 dilution) at room temperature for 1 hour, followed by avidin and biotin block (DAKO Corporation, Carpinteria, CA) for 10 minutes each, and then incubation with biotinylated goat anti-rabbit immunoglobulin G (IgG) (Bio-Rad Laboratories, Hercules, CA) for 20 minutes. Proliferation was assessed by Ki-67 immunostaining. Antigen retrieval was performed in 1× Reveal solution (Biocare Medical, Walnut Creek, CA) and endogenous peroxidase was inhibited by 3% hydrogen peroxide in distilled water. Tissue sections were incubated with an anti-rat Ki-67 mouse monoclonal antibody (clone MIB-5; 1:25 dilution, DAKO) at room temperature for 1 hour, followed by incubation with rat-absorbed goat anti-mouse IgG (Biocare Medical) for 30 minutes. Apoptosis was evaluated by caspase-3 immunostaining. Antigen retrieval was performed in 1× Reveal solution and endogenous peroxidase was inhibited by 3% hydrogen peroxide in distilled water. Tissue sections were incubated at room temperature for 1 hour with a polyclonal antibody (1:100 dilution; Cell Signaling, Beverly, MA) that specifically recognizes the large fragment of activated caspase-3. Specific binding for all stains was amplified using streptavidin horseradish-peroxidase. Chromogen reaction was developed with 3-3′ diaminobenzidine (DAB) solution (DAKO), and nuclei were counterstained with hematoxylin.

Computer-assisted image analysis

For each Ki-67- and caspase-3–stained slide, 2500 nuclei were randomly selected for analysis. For the purposes of this study, the labeling index (LI) for Ki-67 and caspase-3 was defined as: (number of Ki-67- or caspase-3–positive cells/total number of cells) × 100. Ki-67 and caspase-3 LIs were calculated as previously described (19). Briefly, histologic fields were captured with a charge-coupled device (CCD) Sony DKC ST5 camera (Sony, New York, NY) and digitized images were electronically recorded on a computer with a framegrabber board, providing permanent records of the exact specimens evaluated. Images were processed as necessary and then segmented using segmentation techniques such as density and size thresholding with or without dilation and erosion to distinguish negative from positive ob-

jects. The segmentation process results in the generation of binary images. The Optimas 6.5 image analysis software (Optimas, Bothell, WA) generated the measurements of interest and the numerical data were statistically analyzed as described below.

In vitro *growth curve*

Twelve-well plates were seeded with 1×10^3 parental or transduced MATLyLu cells per well. Each cell line was plated in triplicate. Cells were detached with 0.25% trypsin/ethylenediamine tetraacetic acid (EDTA) and counted with a hemocytometer on days 1, 2, 4, 6, and 8.

In vitro *electron microscopy*

Subconfluent parental or transduced MATLyLu cells were detached from T-75 flasks with 0.25% trypsin/EDTA, pelleted by centrifugation at 1000 rpm for 5 minutes at room temperature, and resuspended in 0.01% agarose dissolved in HBSS. Pellets were fixed in 3% glutaraldehyde, 1 M cacodylate buffer, and osmium tetroxide, and then embedded in medcast plastic (Ted Pella Redding, Redding, CA). Ultrathin sections were examined with a Philips 300 transmission electron microscope (FEI, Hillsboro, OR).

Statistical analysis

Numerical data were expressed as means ± the standard error of the mean (SEM). Statistical differences between means for different data sets were evaluated with GraphPad Instat version 3.0 (GraphPad software, San Diego, CA) using one-way analysis of variance (ANOVA) and Tukey-Kramer multiple comparisons test. Statistical significance was indicated by $p < 0.05$.

Results

Decreased growth and slower metastatic progression of MATLyLu-hNIS tumors in Copenhagen rats

Six different *in vivo* experiments were conducted with MATLyLu cells from three different sources (Dr. Laurie K. McCauley, European Collection of Cell Culture [ECACC], and Dr. Albert A. Geldof). Copenhagen rats were subcutaneously injected with either parental MATLyLu cells, MATLyLu cells transduced with vector only (LXSN) retrovirus, or MATLyLu cells transduced with retrovirus expressing the truncated form (hNIS#9) or the full-length form (FLhNIS) of hNIS. Rats were injected with a mixed population of MATLyLu-hNIS cells in four experiments whereas a clonal population was injected in two experiments. In all these experiments, NIS-transduced tumors were significantly smaller than control tumors regardless of the source of the MATLyLu cells, the hNIS construct used to make retrovirus, or whether the tumors were derived from mixed or clonal populations of transduced cells. The results are summarized in Table 1. Initially, rats were injected with either parental cells or a clonal population of MATLyLu-hNIS#9 cells. Although the sample size was small, the three MATLyLu-hNIS#9 tumors were 21-fold smaller than the parental MATLyLu tumor (McCauley, Table 1). Because of the inability to consistently produce lymph node and lung metastases after subcutaneous injection of these parental MATLyLu cells, new MATLyLu cells were obtained from ECACC. In two subsequent *in vivo* experiments, rats were injected with parental MATLyLu cells or a mixed population of MATLyLu-FLhNIS cells. MATLyLu-FLhNIS tumors were 5- to 10-fold smaller than parental tumors in these experiments (ECACC; Table 1). However, the ECACC cells also failed to metastasize consistently after subcutaneous injection. In contrast, lymph node and lung metastases consistently developed when MATLyLu cells obtained from Dr. Geldof were subcutaneously injected in Copenhagen rats, and these cells were used in all subsequent experiments. These MATLyLu cells were transduced with retrovirus expressing LXSN or FLhNIS, and rats were injected with either mixed or clonal populations of transduced cells. MATLyLu-FLhNIS tumors were significantly smaller than control MATLyLu-LXSN tumors (Geldof; Table 1). The differences in tumor size were much more evident when a clonal population (18-fold smaller) of MATLyLu-FLhNIS cells was injected in the rats (Fig. 1) compared to a mixed population (2- to 5-fold smaller).

TABLE 1. hNIS-TRANSDUCED AND CONTROL SUBCUTANEOUS MATLyLu TUMOR VOLUMES IN COPENHAGEN RATS

Experiment	*Tumor type*	*Cell source*	*Clonality*	*Tumor volume (cm^3) mean ± SEM*[a]	*Days post-injection*	*Sample size*	*p value*
1	Parental	McCauley	N/A	15.46 ± 0.0	21	1	N/A
1	hNIS#9	McCauley	Clonal	0.74 ± 0.18	21	3	N/A[b]
2	Parental	ECACC	N/A	1.05 ± 0.21	11	4	N/A
2	FLhNIS	ECACC	Mixed	0.23 ± 0.09	11	4	<0.05
3	Parental	ECACC	N/A	2.20 ± 0.44	10	2	N/A
3	FLhNIS	ECACC	Mixed	0.22 ± 0.03	10	4	<0.001
4	LXSN	Geldof	Mixed	16.25 ± 1.03	21	7	N/A
4	FLhNIS	Geldof	Mixed	7.60 ± 1.32	21	8	<0.001
5	LXSN	Geldof	Mixed	10.60 ± 1.28	18	4	N/A
5	FLhNIS	Geldof	Mixed	2.25 ± 0.73	18	6	<0.01
6	LXSN	Geldof	Clonal	12.77 ± 1.21	22	10	N/A
6	FLhNIS	Geldof	Clonal	0.71 ± 0.15	22	16	<0.001

[a]SEM, standard error of the mean.
[b]Sample size too small for statistical analysis.
hNIS, human sodium iodide symporter.

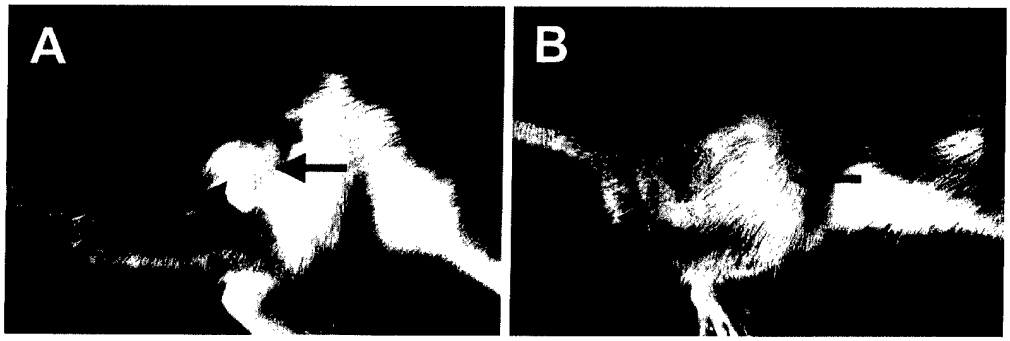

FIG. 1. Appearance of subcutaneous tumors (indicated by arrows) in Copenhagen rats 22 days after injection of a clonal population of MATLyLu-FLhNIS cells (**A**) and MATLyLu-LXSN cells (**B**). The MATLyLu-FLhNIS tumor is significantly smaller than the MATLyLu-LXSN tumor.

Transduced MATLyLu cells from Dr. Geldof metastasized just as consistently as the parental cells with regard to frequency and site; however, the metastatic rate was delayed for LXSN-transduced tumors and even slower for NIS-transduced tumors. Following injection of parental cells, a prominent subcutaneous tumor was palpable by 7 days post-injection (dpi); however, LXSN- and NIS-transduced tumors were barely palpable at this time. Normally, ipsilateral axillary lymph nodes are not palpable in rats. Lymph nodes containing metastatic parental MATLyLu cells (confirmed by histology) were palpable 17 dpi while LXSN or FLhNIS lymph node metastases were not palpable until 21 dpi. Furthermore, rats bearing parental MATLyLu tumors exhibited dyspnea indicative of diffuse pulmonary metastases (confirmed at necropsy) necessitating euthanasia at 24 dpi. In rats bearing MATLyLu-LXSN or MATLyLu-FLhNIS tumors, pulmonary metastases and extensive subcutaneous tumor burden necessitated euthanasia beyond 24 dpi. Rats with mixed LXSN tumors were sacrificed by 32 dpi and those with mixed FLhNIS tumors by 38 dpi, while those with clonal LXSN and FLhNIS tumors were sacrificed by 37 and 46 dpi, respectively.

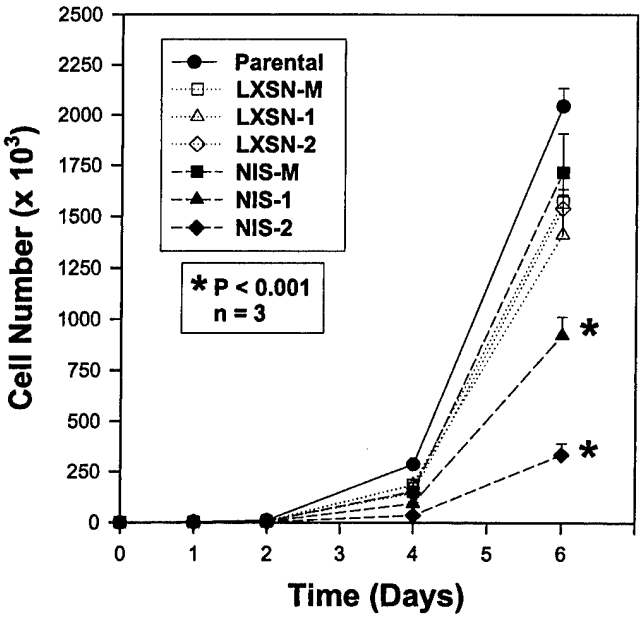

FIG. 2. Growth of parental (solid line) and transduced MATLyLu cells *in vitro*. A mixed population (M) and two different individual clones (1,2) were evaluated for MATLyLu cells transduced with empty vector (LXSN, dotted lines) retrovirus or retrovirus expressing FLhNIS (NIS, dashed lines). Six days post-seeding, a significant difference ($p < 0.001$) in cell number was only apparent between the FLhNIS clones and the parental cells or the LXSN clones. There was no difference *in vitro* between the mixed transduced cells and the parental cells as seen *in vivo*.

Delayed growth In vitro *of clonal FLhNIS cells*

Growth curves were generated by counting parental MATLyLu cells, as well as a mixed population and two dif-

TABLE 2. FLhNIS-TRANSDUCED AND CONTROL MATLyLu SUBCUTANEOUS TUMOR VOLUMES IN ATHYMIC NUDE MICE

Parental MATLyLu[a]	*MATLyLu-FLhNIS-Mixed*
498.47 mm^3	54.98 mm^3
130.90 mm^3	50.27 mm^3
69.12 mm^3	69.12 mm^3
141.37 mm^3	219.90 mm^3
197.92 mm^3	502.66 mm^3
230.91 mm^3	4.19 mm^3
Mean ± SEM[b]:	Mean ± SEM:
211.45 ± 61.81 mm^3	50.19 ± 76.60 mm^3
Mixed MATLyLu-LXSN[c]	*Mixed MATLyLu-FLhNIS*
104.72 mm^3	150.90 mm^3
26.18 mm^3	628.32 mm^3
570.20 mm^3	47.12 mm^3
628.32 mm^3	37.70 mm^3
263.89 mm^3	134.04 mm^3
131.95 mm^3	153.94 mm^3
Mean ± SEM:	Mean ± SEM:
287.54 ± 103.69 mm^3	191.99 ± 89.76 mm^3

[a]One group of mice ($n = 6$) subcutaneously injected in the left flank with parental MATLyLu cells and in the right flank with a mixed population of MATLyLu-FLhNIS cells.

[b]SEM, standard error of the mean.

[c]Second group of mice ($n = 6$) subcutaneously injected in the left flank with a mixed population of MATLyLu-LXSN cells and in the right flank with a mixed population of MATLyLu-FLhNIS cells.

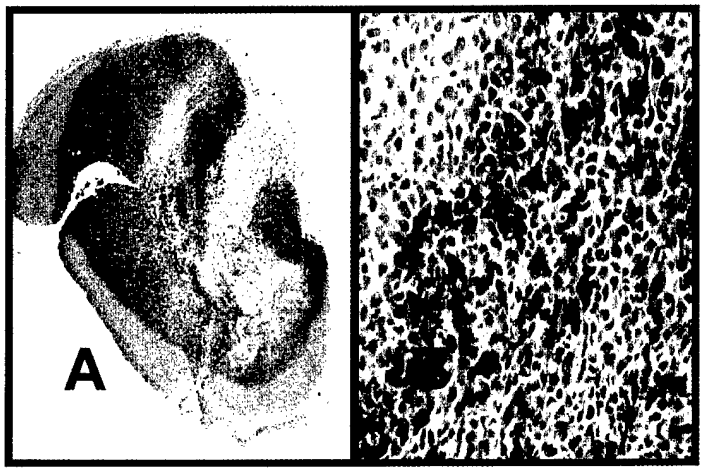

FIG. 3. Immunohistochemical stain for human sodium iodide symporter (hNIS) in a subcutaneous MATLyLu-FLhNIS tumor from an athymic nude mouse. The distribution of NIS-positive cells is characterized by a well-demarcated central region of heterogeneously immunoreactive cells (**A**) circumferentially surrounded by an expansile band of NIS-negative (unstained) cells (20×). The border (**B**) between NIS-positive and NIS-negative cells is distinct. Within the NIS-positive areas, large numbers of MATLyLu-FLhNIS cells with intensely positive membrane staining are interspersed with unstained cells, a staining pattern consistent for tumors that are derived from a mixed population of retrovirally-transduced cells (avidin-biotin complex immunoperoxidase method, hematoxylin counterstain, 200×).

ferent clones of MATLyLu-LXSN and MATLyLu-FLhNIS cells over 8 days to investigate the growth rate of parental and transduced MATLyLu cells *in vitro* (Fig. 2). Cells had reached confluency and were detaching from the wells by 8 days post-seeding. By 6 days post-seeding, a significant difference ($p < 0.001$) in cell number was only apparent between the FLhNIS clones and the parental cells or the LXSN clones; however, there was no difference in the growth rate *in vitro* between the mixed transduced cells and the parental cells in contrast to what was seen *in vivo*.

Variability in the sizes of MATLyLu-FLhNIS tumors in athymic nude mice

Xenografts derived from parental MATLyLu, MATLyLu-LXSN, and MATLyLu-FLhNIS cells were established in athymic nude mice to investigate whether a T-cell–mediated immunologic effect contributed to the difference in growth rates *in vivo* between NIS-transduced and control tumors. All nude mice injected with parental and transduced MATLyLu cells developed prominent, palpable tumors by 7 dpi, but the sizes of NIS-transduced tumors were not consistently smaller or larger than those of parental or vector control tumors (Table 2). Control tumors were larger than FLhNIS tumors in 6 mice, while FLhNIS tumors were larger than control tumors in 5 mice. In 1 mouse, control and FLhNIS tumor sizes were equivalent. Although no statistically significant differences between mixed FLhNIS and control (parental, $p = 0.5476$; mixed LXSN, $p = 0.6967$) tumors were found, tumor volumes were smaller for FLhNIS tumors than control tumors (Table 2).

Outgrowth of NIS-negative cells in tumors derived from a mixed MATLyLu-FLhNIS cell population

The distribution of cells expressing hNIS in tumors derived from a mixed population of MATLyLu-FLhNIS cells

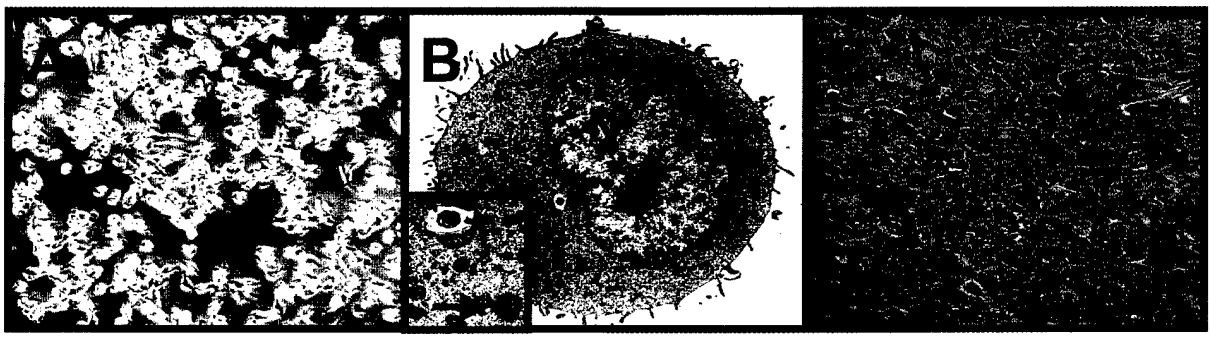

FIG. 4. Morphologic appearance of MATLyLu-FLhNIS cells by phase-contrast microscopy (**A**), transmission electron microscopy (**B**), and light microscopy (**C**). The morphology of parental and MATLyLu-LXSN cells was similar. Ultrastructurally (B), an irregularly round nucleus with a heterochromatic nucleolus, as well as mitochondria (arrow) and rare lysosomes (*) in the cytoplasm are apparent (uranyl acetate and lead citrate, 4859×). Histologically (C), tumor cells are anaplastic with numerous atypical mitotic figures (hematoxylin and eosin, 400×).

in Copenhagen rats and nude mice was evaluated by immunohistochemistry. Interestingly, it was noted that the distribution of NIS-positive cells in the majority of tumors was characterized by a well-demarcated region of heterogeneously immunoreactive cells circumferentially surrounded by an expansile band of NIS-negative (unstained) cells (Fig. 3A). This suggests that cells lacking NIS expression exhibit a growth advantage. As previously reported for tumors that are derived from a mixed population of retrovirally transduced cells, large numbers of MATLyLu-FLhNIS cells with intensely positive membrane staining were interspersed with unstained cells in the NIS-positive areas (Fig. 3B) (3,9).

Decreased proliferation in hNIS-positive areas of rat tumors derived from a mixed MATLyLu-FLhNIS cell population

Proliferation and apoptosis were evaluated by immunostaining tumors derived from mixed populations of MATLyLu-FLhNIS cells in Copenhagen rats (experiment 3) and nude mice for Ki-67 and caspase-3, respectively. The LI for each was compared between hNIS-positive and hNIS-negative areas of the tumors. The Ki-67 LI was significantly lower in hNIS positive areas than hNIS negative areas of mixed rat tumors (positive, 31.25% ± 6.07%; negative, 43.75% ± 6.62%; $p < 0.05$; $n = 5$). There were no significant differences in the caspase-3 LI between the two areas in rat tumors (positive, 7.37% ± 3.45%; negative, 13.37% ± 5.77%; $p = 0.3638$; $n = 5$), or in the LIs for Ki-67 (positive, 84.35% ± 5.47%; negative, 85.61% ± 5.78%); $p = 0.7693$; $n = 6$) or caspase-8 (positive, 1.59% ± 0.86%; negative, 1.01% ± 0.27%; $p = 0.5165$; $n = 6$) in nude mouse tumors.

No effect on differentiation of MATLyLu cells by NIS

In order to investigate whether exogenous hNIS expression induces differentiation of the anaplastic MATLyLu cells, microscopic morphology of the tumor cells *in vitro* and *in vivo*, as well as ultrastructural morphology *in vitro* was evaluated. There were no differences in morphology by phase contrast microscopy, transmission electron microscopy, or light microscopy between parental, LXSN-transduced and hNIS-transduced MATLyLu cells. Representative cells are illustrated in Figure 4.

Discussion

The results of this study clearly demonstrate that growth of MATLyLu cells expressing exogenous hNIS is decreased *in vitro* and *in vivo*. Subcutaneous tumors were smaller and metastatic progression was slower in Copenhagen rats injected with MATLyLu-hNIS cells. This effect on *in vivo* growth was consistently observed in six different experiments and occurred independent of the source of MATLyLu cells, the hNIS construct used to generate retrovirus, and whether the tumors were derived from mixed or clonal populations of transduced cells. MATLyLu-FLhNIS tumors in nude mice had a lower, albeit not statistically significant, growth rate than control tumors. Growth of the clonal populations of NIS-transduced cells was significantly decreased compared to parental or clonal LXSN-transduced cells *in vitro*. Furthermore, the pattern of hNIS immunohistochemical staining in Copenhagen rat and nude mouse tumors derived from mixed populations of MATLyLu-FLhNIS cells demonstrated that NIS-positive cells were confined to a central defined region surrounded by a band of NIS-negative cells.

Although previous studies investigating the utility of NIS gene transfer to facilitate radioiodide therapy for various cancers have not reported overt differences in growth between NIS-positive and NIS-negative tumors, Haberkorn et al. (5) and Shimura et al. (7) reported reduced weights of hNIS- and rNIS-expressing tumors compared to parental tumors in syngeneic rats, suggesting a similar effect. In addition, axillary lymph node metastases were previously only detected by nuclear scintigraphy in 3 of 12 rats injected with a mixed population of MATLyLu-FLhNIS cells, and NIS expression was absent by immunohistochemistry in the remaining lymph nodes (9). Taken together, these data suggest that MATLyLu cells lacking hNIS expression within a mixed population exhibit a growth advantage over NIS-expressing cells.

Possible mechanisms contributing to this *in vivo* growth difference include a direct effect by NIS on cell growth by decreasing proliferation, increasing apoptosis, and/or inducing cell cycle arrest. A decrease in proliferation was supported by the immunohistochemical results for Ki-67 in mixed MATLyLu-FLhNIS rat tumors, in which the Ki-67 LI was decreased in NIS-positive areas compared to the surrounding NIS-negative areas. Increased apoptosis was not evident by caspase-3 immunostaining, and pyknotic nuclei/apoptotic bodies were not apparent on histologic evaluation of MATLyLu-hNIS tumors. In addition to inducing apoptosis through a p53-independent mechanism (20,21), excess iodide has been shown to inhibit growth of FRTL-5 rat thyroid cells through cell cycle arrest (22–24).

NIS is a marker of differentiation in the thyroid gland (1,25,26). This is evidenced by the fact that avidity for radioiodide is positively correlated with NIS expression and differentiation in thyroid cancer (27–29). The presence of NIS in transduced MATLyLu tumors may be causing the anaplastic MATLyLu cells to become more differentiated. However, the histologic and ultrastructural morphology of MATLyLu-FLhNIS cells *in vitro* and *in vivo* was indistinguishable from that of MATLyLu-LXSN or parental cells. Tumors were equally anaplastic with numerous mitotic figures and comparable regions of necrosis. Subcutaneous MATLyLu-FLhNIS tumors also metastasized with the same frequency and to identical sites (ipsilateral regional lymph nodes, axillary lymph node, and lungs) as control tumors, just at later times. It is also unlikely that the constitutive transport of two Na^+ ions with one I^- ion has any adverse effect on cellular homeostasis because the sodium gradient is maintained by a Na^+/K^+ pump (1).

The fact that MATLyLu-hNIS tumors were consistently smaller than control tumors in immunocompetent syngeneic rats but were not always smaller than control tumors in immunodeficient mice suggests that an immunologic effect may also be contributing to the decreased growth of MATLyLu-hNIS tumors *in vivo*. Possible sources of immunogenicity in this study include the xenogeneic cell lines, the retroviral vector, in particular the neomycin resistance gene, and hNIS. NIS is an endogenous gene pres-

ent in numerous tissues in addition to the thyroid gland such as salivary glands, gastric mucosa, lactating mammary gland, kidney, and placenta (30–36). Although human NIS shares 84% identity with rat and mouse NIS (37,38), it has been identified as an autoantigen in patients with autoimmune thyroid disease (39,40). Despite this, growth of MATLyLu-hNIS tumors in Copenhagen rats and nude mice was not associated with an inflammatory cell response at either the primary or metastatic sites. However, this does not exclude the role of a humoral response. These animals have extensive tumor burdens, and numerous cytokines are likely to be elevated.

A final mechanism that must be considered is the effect of retroviral integration on the growth rate differences. Retroviral vectors are attractive methods of gene delivery because they stably integrate into the chromosome providing for long-term expression (12,41). The process of integration, which is random, involves a prefatory cleavage reaction and a subsequent strand-transfer reaction (42). Depending on the site of integration of retrovirus expressing hNIS, various *cis*-acting elements may be modulating the expression of hNIS. Such an explanation would be likely if the growth rate differences *in vivo* were only apparent with a clonal population of hNIS-transduced cells, as was observed *in vitro*. However, the differences in growth were also consistently seen in four different *in vivo* experiments using a mixed population of hNIS-transduced cells.

This study indicates that exogenous NIS expression causes decreased growth of subcutaneous MATLyLu tumors and slower metastatic progression, although the exact mechanism for this effect remains to be elucidated. Investigators need to be aware of these growth rate differences between tumors with and without hNIS expression in the absence of radioiodide treatment. Such growth rate differences make interpretation of tumor regression, metastatic progression, and animal survival after radioiodide therapy difficult, and emphasize the need for the inclusion of appropriate treatment and vector controls. This decreased growth could provide an additional potential benefit of NIS-mediated gene therapy for the treatment of cancer.

Acknowledgments

We thank Dr. Albert Geldof and Dr. Laurie McCauley for the MATLyLu cells; Dr. Kathleen Boris-Lawrie for the LXSN retroviral vector; Ms. Anjli Venkateswaran, Ms. Danielle Westfall, and Mr. Marc Lavender for assistance with animal injections and postmortem evaluations; Dr. Richard Kloos for scientific discussion; Ms. Kathy Hopwood for animal husbandry; Mr. Alan Flechtner and Ms. Anne Saulsbery for histology slide preparation; Ms. Evelyn Handley and Ms. Mary Gessford for electron microscopy and immunohistochemistry support, respectively; and, Ms. Heather Caprette and Mr. Marc Hardman for assistance with photography and figure illustrations.

This project was supported in part by a fellowship from the Schering-Plough Research Institute (K.M.D.L., C.C.C.), Institutional National Research Service Award T32 CA09228-23 from The Ohio State University, Comprehensive Cancer Center, Department of Internal Medicine, Division of Hematology and Oncology (K.M.D.L.), and U.S. Army Medical Research and Material Command Department of Defense 2001 Prostate Cancer Research Program PC010162 (S.M.J.).

References

1. Carrasco N 1993 Iodide transport in the thyroid gland. Biochim Biophys Acta **1154**:65–82.
2. Mazzaferri EL 2000 Carcinoma of follicular epithelium: Radioiodine and other treatments and outcomes. In: Braverman LE, Utiger RD (eds) Werner and Ingbar's The Thyroid: A Fundamental and Clinical Text. Lippincott Williams and Wilkins, Philadelphia, pp. 904–929.
3. Boland A, Ricard M, Opolon P, Bidart J-M, Yeh P, Filetti S, Schlumberger M, Perricaudet M 2000 Adenovirus-mediated transfer of the thyroid sodium/iodide symporter gene into tumors for a targeted radiotherapy. Cancer Res **60**:3484–3492.
4. Nakamoto Y, Saga T, Misaki T, Kobayshi H, Sato N, Ishimori T, Kosugi S, Sakahara H, Konishi J 2000 Establishment and characterization of a breast cancer cell line expressing Na+/I− symporters for radioiodide concentrator gene therapy. J Nucl Med **41**:1898–1904.
5. Haberkorn U, Henze M, Altmann A, Jiang S, Morr I, Mahmut M, Peschke P, Kübler W, Debus J, Eisenhut M. Transfer of the human Nal symporter gene enhances iodide uptake in hepatoma cells. J Nucl Med **42**:317–325.
6. Mandell RB, Mandell LZ, Link CJ Jr 1999 Radioisotope concentrator gene therapy using the sodium/iodide symporter gene. Cancer Res **59**:661–668.
7. Shimura H, Haraguchi K, Miyazaki A, Endo T, Onaya T 1997 Iodide uptake and experimental 131I therapy in transplanted undifferentiated thyroid cancer cells expressing the Na+/I− symporter gene. Endocrinology **138**:4493–4496.
8. Smit JW, Schröder-van der Elst JP, Karperien M, Que I, Stokkel M, van der Heide D, Romijn JA 2002 Iodide kinetics and experimental (131)I therapy in a xenotransplanted human sodium-iodide symporter-transfected human follicular thyroid carcinoma cell line. J Clin Endocrinol Metab **87**:1247–1253.
9. La Perle KMD, Shen D, Buckwalter TLF, Williams B, Haynam A, Hinkle G, Pozderac G, Capen CC, Jhiang SM 2002 In vivo expression and function of the sodium iodide symporter following gene transfer in the MATLyLu rat model of metastatic prostate cancer. Prostate **50**:170–178.
10. Spitzweg C, O'Connor MK, Bergert ER, Tindall DJ, Young CY, Morris JC 2000 Treatment of prostate cancer by radioiodine therapy after tissue-specific expression of the sodium iodide symporter. Cancer Res **60**;6526–6530.
11. Spitzweg C, Dietz AB, O'Connor MK, Bergert ER, Tindall DJ, Young CYF, Morris JC 2001 In vivo sodium iodide symporter gene therapy of prostate cancer. Gene Ther **8**:1524–1531.
12. Miller A, Rosman G 1989 Improved retroviral vectors for gene transfer and expression. Biotechniques **7**:980–990.
13. Dunning W 1963 Prostate cancer in the aging rat. Monogr Natl Cancer Inst **12**;351–369.
14. Isaacs JT, Yu GW, Coffey DS 1981 The characterization of a newly identified, highly metastatic variety of Dunning R 3327 rat prostatic adenocarcinoma system: The MAT LyLu tumor. Invest Urol **19**:20–23.
15. Geldof AA, Rao BR 1990 Factors in prostate cancer metastasis. Anticancer Res **10**:1303–1306.
16. Vieweg J, Heston WD, Gilboa E, Fair WR 1994 An experimental model simulating local recurrence and pelvic lymph node metastasis following orthotopic induction of prostate cancer. Prostate **24**:291–298.
17. Janik P, Briand P, Hartmann NR 1975 The effect of estrone-

progesterone treatment on cell proliferation kinetics of hormone-dependent GR mouse mammary tumors. Cancer Res **35**:3698–3704.
18. Jhiang SM, Cho JY Ryu KY, DeYoung BR, Smanik PA, McGaughy VR, Fischer AH, Mazzaferri EL 1998 An immunohistochemical study of Na+/I− symporter in human thyroid tissues and salivary gland tissues. Endocrinology **139**:4416–4419.
19. Baron DA, La Perle KMD, Blomme EAG 2000 The use of computer-assisted image analysis in the evaluation of preclinical tumor efficacy models. Curr Opin Drug Discov Devel **3**:79–93.
20. Burikhanov RB, Matsuzaki S 2000 Excess iodine induces apoptosis in the thyroid of goitrogen-pretreated rats in vivo. Thyroid **10**:123–129.
21. Vitale M, Di Matola T, D'Ascoli F, Salzano S, Bogazzi F, Fenzi G, Martino E, Rossi G 2000 Iodide excess induces apoptosis in thyroid cells through a p53-independent mechanism involving oxidative stress. Endocrinology **141**:598–605.
22. Saji M, Isozaki O, Tsushima T, Arai M, Miyakawa M, Ohba Y, Tsuchiya Y, Sano T, Shizume K 1988 The inhibitory effect of iodide on growth of rat thyroid (FRTL-5) cells. Acta Endocrinol (Copenh) **119**:145–151.
23. Becks GP, Eggo MC, Burrow GN 1988 Organic iodine inhibits deoxyribonucleic acid synthesis and growth in FRTL-5 thyroid cells. Endocrinology **123**:545–551.
24. Smerdely P, Pitsiavas V, Boyages SC 1993 Evidence that the inhibitory effects of iodide on thyroid cell proliferation are due to arrest of the cell cycle at G0G1 and G2M phases. Endocrinology **133**:2881–2888.
25. Damante G, Di Lauro R 1994 Thyroid-specific gene expression. Biochim Biophys Acta **1218**:255–266.
26. Lazar V, Bidart JM, Caillou B, Mahe C, Lacroix L, Filetti S, Schlumberger M 1999 Expression of the Na+/I− symporter gene in human thyroid tumors: A comparison study with other thyroid-specific genes. J Clin Endocrinol Metab **84**:3228–3234.
27. Caillou B, Troalen F, Baudin E, Talbot M, Filetti S, Schlumberger M, Bidart JM 1998 Na+/I− symporter distribution in human thyroid tissues: An immunohistochemical study. J Clin Endocrinol Metab **83**:4102–4106.
28. Min JJ, Chung GK, Lee YJ, Jeong JM, Lee DS, Jang JJ, Lee MC, Cho BY 2001 Relationship between expression of the sodium/iodide symporter and 131I uptake in recurrent lesions of differentiated thyroid carcinoma. Eur J Nucl Med **28**:639–645.
29. Castro MR, Bergert ER, Goellner JR, Hay ID, Morris JC 2001 Immunohistochemical analysis of sodium iodide symporter expression in metastatic differentiated thyroid cancer: Correlation with radioiodine uptake. J Clin Endocrinol Metab **86**:5627–5632.
30. Spitzweg C, Joba W, Eisenmenger W, Heufelder AE 1998 Analysis of human sodium iodide symporter gene expression in extrathyroidal tissues and cloning of its complementary deoxyribonucleic acids from salivary gland, mammary gland, and gastric mucosa. J Clin Endocrinol Metab **83**:1746–1751.
31. Jhiang SM 2000 Regulation of sodium/iodide symporter. Rev Endocr Metab Disord **1**:205–215.
32. Perron B, Rodriguez AM, Leblanc G, Pourcher T 2001 Cloning of the mouse sodium iodide symporter and its expression in the mammary gland and other tissues. J Endocrinol **170**:185–196.
33. Tazebay UH, Wapnir IL, Levy O, Dohan O, Zuckier LS, Zhao QH, Deng HF, Amenta PS, Fineberg S, Pestell RG, Carrasco N 2000 The mammary gland iodide transporter is expressed during lactation and in breast cancer. Nat Med **6**:871–878.
34. Kotani T, Ogata Y, Yamamoto I, Aratake Y, Kawano JI, Suganuma T, Ohtaki S 1998 Characterization of gastric Na+/I− symporter of the rat. Clin Immunol Immunopathol **89**: 271–278.
35. Mitchell AM, Manley SW, Morris JC, Powell KA, Bergert ER, Mortimer RH 2001 Sodium iodide symporter (NIS) gene expression in human placenta. Placenta **22**:256–258.
36. Spitzweg C, Dutton CM, Castro MR, Bergert ER, Goellner JR, Heufelder AE, Morris JC 2001 Expression of the sodium iodide symporter in human kidney. Kidney Int **59**:1013–1023.
37. Smanik PA, Liu Q, Furminger TL, Ryu K, Xing S, Mazzaferri EL, Jhiang SM 1996 Cloning of the human sodium iodide symporter. Biochem Biophys Res Commun **226**:339–345.
38. Pinke LA, Dean DS, Bergert ER, Spitzweg C, Dutton CM, Morris JC 2001 Cloning of the mouse sodium iodide symporter. Thyroid **11**:935–939.
39. Endo T, Kogai T, Nakazato M, Saito T, Kaneshige M, Onaya T 1996 Autoantibody against Na+/I− symporter in the sera of patients with autoimmune thyroid disease. Biochem Biophys Res Commun **224**:92–95.
40. Endo T, Kaneshige M, Nakazato M, Kogai T, Saito T, Onaya T 1996 Autoantibody against thyroid iodide transporter in the sera from patients with Hashimoto's thyroiditis possesses iodide transport inhibitory activity. Biochem Biophys Res Comm **228**:199–202.
41. Anderson WF 1998 Human gene therapy. Nature **392**:25–30.
42. Hindmarsh P, Leis J 1999 Retroviral DNA integration. Microbiol Mol Biol Rev **63**:836–843.

Address reprint requests to:
Sissy M. Jhiang, Ph.D.
The Ohio State University
Department of Physiology and Cell Biology
304 Hamilton Hall
1645 Neil Avenue
Columbus, OH 43210

E-mail: Jhiang.1@osu.edu

Appendix 2

Gene Therapy (2004) 11, 161–169

www.nature.com/gt

RESEARCH ARTICLE

Effects of dose, intervention time, and radionuclide on sodium iodide symporter (NIS)-targeted radionuclide therapy

DHY Shen[1,6], DK Marsee[1], J Schaap[1], W Yang[2], J-Y Cho[1], G Hinkle[3], HN Nagaraja[4], RT Kloos[3,5], RF Barth[2] and SM Jhiang[1,5]

[1]Department of Physiology and Cell Biology, College of Medicine and Public Health, The Ohio State University, Columbus, OH, USA; [2]Department of Pathology, College of Medicine and Public Health, The Ohio State University, Columbus, OH, USA; [3]Department of Radiology, College of Medicine and Public Health, The Ohio State University, Columbus, OH, USA; [4]Department of Statistics, College of Medicine and Public Health, The Ohio State University, Columbus, OH, USA; [5]Department of Internal Medicine, College of Medicine and Public Health, The Ohio State University, Columbus, OH, USA; and [6]Department of Nuclear Medicine, Tri-Service General Hospital, National Defense Medical Center, Taipei, ROC

The sodium iodide symporter (NIS) mediates iodide uptake into thyrocytes and is the molecular basis of thyroid radioiodine therapy. We previously have shown that NIS gene transfer into the F98 rat gliomas facilitated tumor imaging and increased survival by radioiodine. In this study, we show that: (1) the therapeutic effectiveness of ^{131}I in prolonging the survival time of rats bearing F98/hNIS gliomas is dose- and treatment-time-dependent; (2) the number of remaining NIS-expressing tumor cells decreased greatly in RG2/hNIS gliomas post ^{131}I treatment and was inversely related to survival time; (3) 8 mCi each of $^{125}I/^{131}I$ is as effective as 16 mCi ^{131}I alone, despite a smaller tumor absorbed dose; (4) $^{188}ReO_4$, a potent β^- emitter, is more efficient than ^{131}I to enhance the survival of rats bearing F98/hNIS gliomas. These studies demonstrate the importance of radiopharmaceutical selection, dose, and timing of treatment to optimize the therapeutic effectiveness of NIS-targeted radionuclide therapy following gene transfer into gliomas.
Gene Therapy (2004) **11**, 161–169. doi:10.1038/sj.gt.3302147

Keywords: *sodium iodide symporter; radionuclide therapy; brain neoplasm*

Introduction

The sodium iodide symporter (NIS) is a membrane glycoprotein that mediates iodide uptake in the thyroid gland and several extrathyroid tissues. NIS-mediated radioiodide uptake into thyroid epithelial cells is the molecular basis of thyroidal radioiodine therapy. The differential radioiodide accumulation in thyrocytes is further enhanced by the presence of iodide organification in thyroid tissues. Furthermore, iodide uptake/organification can be increased selectively in thyroid tissues by elevated serum thyrotropin levels. Consequently, most administered radioiodine is targeted to thyroid tissues, and radioiodine has been very effective in treating thyroid cancer, hyperthyroidism, and goiter.

Since the cloning of NIS,[1,2] many investigators have explored the ability of NIS gene transfer to facilitate targeted radioiodide therapy in nonthyroidal cancers. NIS gene transfer has been demonstrated to increase radioactive iodine uptake (RAIU) up to several hundred-fold in a variety of cell types.[3–6] In addition to allowing *in vivo* tumor imaging,[5–9] NIS gene transfer into tumor cells also renders them susceptible to being killed *in vitro* by ^{131}I.[4,10,11] However, lack of iodine organification in NIS-transduced tumors has raised concerns about the ultimate effectiveness of NIS-mediated radionuclide therapy for nonthyroidal malignancies, as an insufficient tumor radiation absorbed dose[8,9] may result from short radionuclide retention time. Nevertheless, an NIS-transduced prostatic tumor xenograft in mice was decreased in size by a single 3 mCi dose of ^{131}I injected intraperitoneally.[12]

We hypothesized that NIS-mediated radionuclide therapy would be useful to treat tumors such as gliomas, which are currently limited by a narrow radiation therapeutic window. At least 55 Gy of external radiation is required to achieve tumor control; however, patients often developed normal brain tissue necrosis when more than 60 Gy of radiation is delivered solely by external radiation.[13–15] Although numerous strategies have been developed to increase the tumor-absorbed dose while minimizing radiation to normal brain tissues, thus far most of these attempts have proven unsatisfactory. Interstitial brachytherapy by physical placement of radionuclides in or near the tumor cannot differentiate microscopic tumors, from surrounding normal brain tissues,[16] as evidenced by a high incidence of

Correspondence: Dr SM Jhiang, Department of Physiology and Cell Biology, The Ohio State University, 304 Hamilton Hall, 1645 Neil Avenue, Columbus, OH 43210-1218, USA
Received 14 April 2003; accepted 25 July 2003

symptomatic brain necrosis developing in patients treated with interstitial brachytherapy.[13,17] Another strategy, radioimmunotherapy (RIT), has several limitations, including unwanted immunocomplex formation of radiolabeled antibody to nontumor tissues[18,19] and the difficulty in delivering radiolabeled antibody across the blood–brain barrier (BBB). The differential distribution of radiolabeled antibody between tumors and normal tissues is often not satisfactory for targeted radionuclide therapy.[20] As shown in phase II–III clinical trials, locoregional administration of radiolabeled antibody into surgical cavities following tumor resection has modestly improved survival.[21–24] However, many challenges exist to extend RIT to routine practice. For example, nonselective radiation to normal parenchyma, poor penetration of radiolabeled antibody into bulky tumors, and the complexity of the radiolabeling procedure remain as hurdles to the success of RIT in treating gliomas.

NIS-mediated radionuclide therapy has several features that make it an attractive approach for the treatment of patients with gliomas. Since glioma-targeted NIS gene transfer facilitates higher radionuclide accumulation in gliomas compared to the surrounding normal brain tissues, the differential radiation exposure between gliomas and normal brain tissues can be broadened. Furthermore, complex radiolabeling procedures are not required for NIS-mediated radionuclide therapy, since many NIS substrates have radioactive isotopes. Finally, the small sizes of NIS radioactive substrates should result in both increased penetration of the BBB and better diffusion capacity within the tumor compared to radiolabeled monoclonal antibodies. In our previous study, we showed that *ex vivo* NIS gene transfer to F98 rat glioma cells conferred a moderate survival benefit in ^{131}I-treated rats bearing intracerebral F98/hNIS gliomas.[5] In the present study, we show that the ^{131}I therapeutic effectiveness is dose-dependent and influenced by intervention time. To validate NIS-targeted radionuclide therapy in another glioma animal model, we have demonstrated therapeutic effectiveness of ^{131}I in rats carrying intracerebral RG2/hNIS gliomas. Finally, the therapeutic contributions of ^{125}I and $^{188}ReO_4$ in NIS-targeted radionuclide therapy are investigated.

Results

^{131}I therapeutic effectiveness is dose-dependent and influenced by intervention time

To investigate whether ^{131}I therapeutic effectiveness is dose-dependent, several therapeutic trials of different ^{131}I doses were conducted. As shown in Table 1, all treated rats appear to have improved survival compared to untreated rats. Statistical analysis using a two-sample *t*-test with unequal variance assumption showed that only the survival of rats treated with 16 mCi was significantly prolonged. In order to compare therapeutic effectiveness among different trials, the percentage of increased life span (%ILS) of treated rats with various doses of ^{131}I was calculated (see 'statistics' section in Materials and methods). There was a linear dose-dependent increase of %ILS for administered doses of ^{131}I (R=0.91). Similarly, the level of significance for improved survival, as indicated by *P*-value, increased with higher doses of ^{131}I.

To investigate the effect of intervention time on therapeutic effectiveness, 16 mCi of ^{131}I was administered to rats bearing F98/hNIS glioma either 14 or 22 days post tumor implantation (DPI). Compared to the untreated rats, which had a mean survival time (MST) of

Table 1 Dose regimen of radionuclide treatment and survival of F98/hNIS glioma-bearing rats

Experiment	*Radionuclide*	*Total dose (mCi)*	*Rx. time (day)*	*Survival (DPI)*		*% ILS*	*P-value*
				Untreated rats	*Treated rats*		
Dose-dependency	^{131}I	4	14	35.3±3.3 (N=6)	41.0±10.8 (N=6)	16.1	0.26
	^{131}I	5.6	14	34.7±4.5 (N=3)	42.0±9.9 (N=4)	21	0.25
	^{131}I	5.6	14	29.3±3.5 (N=3)	35.5±6.4 (N=4)	21.2	0.16
	^{131}I	8	14	29.3±3.5 (N=3)	39.8±10.6 (N=4)	35.8	0.14
	^{131}I	8	14	34.7±4.5 (N=3)	48.7±6.8 (N=3)	40.3	0.049
	^{131}I	16	14	35.3±3.3 (N=6)	54.9±9.9 (N=7)	55.5	0.0014
	^{131}I	16	14	38.0±1.0 (N=3)	55.1±11.7 (N=8)	45	0.0043
Intervention time	^{131}I	16	14	38.0±1.0 (N=3)	55.1±11.7 (N=8)	45	0.0043
	^{131}I	16	22		45.0±4.1 (N=8)	16.6	0.0034
^{125}I *versus* ^{131}I *versus* ^{125}I/^{131}I cocktail	^{131}I	16[a]	13,14	34.4±1.9 (N=7)	47.3±8.5 (N=6)	32.4	0.0127
	^{125}I	16[a]	13,14		39.2±4.0 (N=6)	14.7	0.0337
	^{131}I+^{125}I	8[a] and 8[a]	13,14		46.7±5.4 (N=6)	30.9	0.0019
$^{188}ReO_4$ *versus* ^{131}I	$^{188}ReO_4$	8	14	34.7±4.5 (N=3)	61.8±10.5 (N=4)	78.1	0.0084
	^{131}I	8	14		48.7±6.8 (N=3)	40.3	0.0492
	$^{188}ReO_4$	8	14	29.3±3.5 (N=3)	44.3±7.1 (N=4)	51.2	0.0177
	^{131}I	8	14		39.8±10.6 (N=4)	35.8	0.0222

The total dose was divided into two fractions with 12 h apart, unless otherwise indicated. Rx. time (day) indicates the day post tumor implantation when radionuclide was administered. Survival time is presented as mean±s.d. days post tumor implantation (DPI). Percentage of increased life span (%ILS) is calculated as the difference between the MST of radionuclide-treated and untreated groups, divided by the MST of the untreated group. *P*-values were calculated using a two-sample *t*-test with unequal variance assumption.
[a]The dose was administered in three fractions.

38.0±1.0 DPI, the survival times for rats treated at 14 and 22 DPI were 55.1±11.7 and 44.3±4.3 DPI, respectively (Table 1). The therapeutic effectiveness of early intervention (45% ILS) was greater than later intervention (16.6% ILS). The tumor size of intracerebral F98/hNIS gliomas 14 DPI was barely detectable by either imaging or postmortem examination, compared to approximately 2 mm^3 at 22 DPI (data not shown).

NIS-targeted ^{131}I therapy is validated in another animal model carrying intracerebral RG2/hNIS gliomas

To validate NIS-targeted radioiodine therapy in an alternative animal model, the therapeutic effectiveness of ^{131}I was investigated in rats bearing intracerebral RG2/hNIS gliomas. RG2/hNIS cells had nine-fold higher RAIU than F98/hNIS cells *in vitro* (data not shown). Serial ^{123}I imaging showed higher radioiodine uptake in RG2/hNIS than F98/hNIS gliomas, with similar tumor radioiodine retention time (Figure 1). Temporal analysis of *ex vivo* gamma counting of RG2/hNIS gliomas showed that radioiodine accumulation remained high up to 12 h post ^{125}I injection, with an average uptake value of 6.4–8.7% ID/g (Table 2). In comparison, at the same time point, the average uptake value of RG2 gliomas carrying empty vector (RG2/LXSN) was 0.06–0.67% ID/g, and that of normal brain tissues was 0.03–0.16% ID/g. Thus, NIS gene transfer into RG2 gliomas increased ^{125}I accumulation more than 70-fold, compared with normal brain tissue. The biological half-life of radioiodine in RG2/hNIS tumors was approximately 19.6 h, as determined by time activity curve (TAC) of ^{125}I in RG2/hNIS gliomas (Figure 3B). A similar biological half-life was estimated by serial ^{123}I scintigraphy (Figure 1).

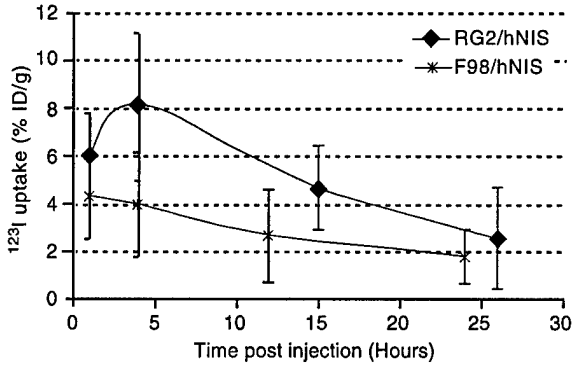

Figure 1 Serial ^{123}I planar imaging showed higher radioiodine uptake in RG2/hNIS than F98/hNIS gliomas. Rats implanted with NIS-transduced gliomas intracerebrally were subjected to imaging studies when the tumor size approximated 3–6 mm in diameter (N=3 per group. Tumor ^{123}I uptake was calculated by measuring the count rates in tumor region and calibrated by a known standard ^{123}I dose. Tumor mass was determined by weighing the tumor after completion of imaging. The data are presented as a percentage of injected dose per gram (%ID/g) of tumor. There was a similar ^{123}I retention time (a biological half-life of 15–20 h) in tumors for both NIS-transduced gliomas.

The MST of rats bearing RG2/hNIS gliomas treated with 16 mCi of ^{131}I on D14 (Table 3) was significantly different from the other groups at 5% level of significance (one-way ANOVA with Dunnett's test). There was no significant difference in the survival time among untreated rats bearing parental RG2 gliomas, untreated rats bearing RG2/LXSN gliomas, untreated rats bearing RG2/hNIS gliomas, and ^{131}I-treated rats bearing RG2/LXSN gliomas. All rats bearing RG2-derived gliomas had approximately the same tumor sizes with similar histology when euthanized for moribund signs. Immunohistochemical staining against NIS revealed that ^{131}I-treated RG2/hNIS gliomas had either reduced numbers or an absence of NIS-expressing cells compared to untreated RG2/hNIS gliomas (Figure 2a). The number of NIS-expressing cells remaining in the tumors appeared inversely related to survival time of ^{131}I-treated rats bearing RG2/hNIS gliomas (Figure 2b). The degree of reduction in NIS-expressing cells in ^{131}I-treated F98/hNIS gliomas compared to untreated tumors was less obvious (Figure 2a).

^{131}I and combined $^{125}I/^{131}I$ treatment had similar therapeutic effectiveness in prolonging the survival time of rats bearing F98/hNIS gliomas

Isotopes of radioiodine emit different energy particles. To investigate the therapeutic efficacy of an Auger emitter and the possible synergistic effect of combined Auger electron and β^- emissions, rats bearing F98/hNIS gliomas were treated with ^{125}I, or with ^{125}I and ^{131}I, compared to ^{131}I alone. As shown in Table 1, all radioiodine-treated rats had prolonged survival times compared to untreated rats. However, only the MST of ^{131}I- and combined $^{125}I/^{131}I$-treated rats bearing F98/hNIS gliomas was significantly longer than that of the untreated group (5% level of significance, one-way ANOVA with Dunnett's test). Thus, with the same radioactivity administered on days 13 and 14 post tumor

Table 2 Temporal profile of *ex vivo* ^{125}I accumulation in RG2 gliomas

Tissues	*^{125}I uptake (%ID/g) at different time post ^{125}I injection*				
	30 s	*2 h*	*4–6 h*	*12 h*	*24 h*
RG2/hNIS					
Tumor	7.0±1.8	7.9±1.5	8.7±1.7	6.4±2.8	2.5±1.6
Adjacent Brain	0.14±0.1	0.15±0.1	0.12±0.1	0.03±0.0	0.00±0.0
RG2/LXSN					
Tumor	0.67±0.3	0.24±0.2	0.12±0.0	0.06±0.0	0.02±0.0
Adjacent Brain	0.16±0.1	0.11±0.0	0.10±0.1	0.07±0.0	0.01±0.0

The ^{125}I accumulation from RG2 gliomas and adjacent normal brain tissue is presented as a percentage of injected dose per gram of tissue (%ID/g) and as mean±s.d. from three rats at each time point.

Table 3 Survival of RG2 glioma-bearing rats

Group	*Gene transduction*	*^{131}I treatment*	*Survival (DPI)*
Parental RG2	None	None	24.0±1.4 (*N*=7)
RG2/LXSN	Empty vector	None	24.6±0.5 (*N*=5)
RG2/LXSN	Empty vector	16 mCi	23.9±3.1 (*N*=7)
RG2/hNIS	hNIS	None	24.0±4.5 (*N*=7)
RG2/hNIS	hNIS	16 mCi	30.2±5.1 (*N*=10)

Survival time is presented as mean±s.d. days post tumor implantation (DPI). Total dose of ^{131}I treatment was divided into two fractions with 12 h apart.

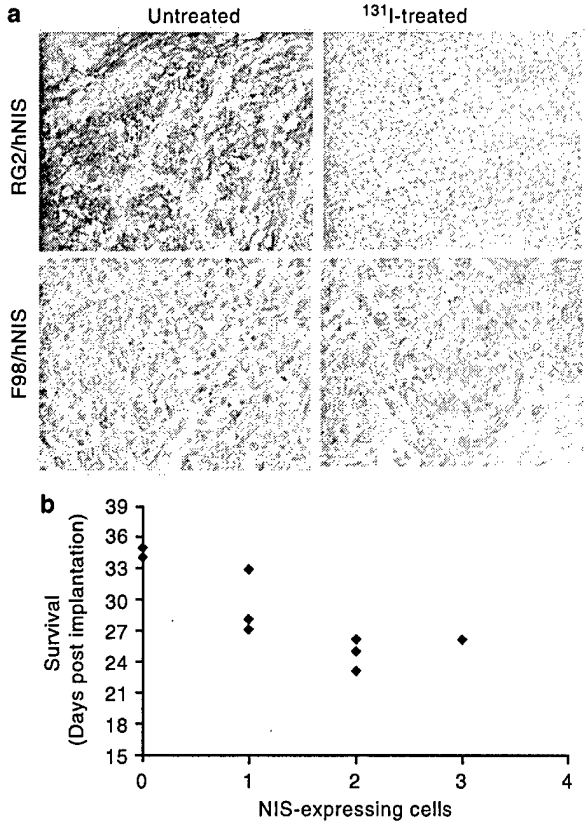

Figure 2 Anti-hNIS IHC staining of post-mortem tumors. (a) Anti-hNIS IHC staining of tumor sections shows reduced numbers of NIS-expressing tumor cells in ^{131}I-treated RG2/hNIS gliomas (right upper panel), compared to untreated controls (left upper panel). In comparison, the reduction is not pronounced between untreated and ^{131}I-treated F98/hNIS gliomas (left and right lower panels). Following implantation with 1×10^3 hNIS-transduced glioma cells, rats were either untreated or given 16 mCi of ^{131}I on day 14 post tumor implantation ($N \geq 6$ per group). (b) Inverse relationship between the remaining NIS-expressing cells in tumors and survival times of ^{131}I-treated rats bearing RG2/hNIS gliomas is demonstrated. The percentage of NIS-expressing cells in a whole tumor was estimated by the scale of 0–4 (0: 0%, 1: 25%, 2: 50%, 3: 75%, and 4: 100%). The survival time is presented as days post tumor implantation (DPI).

implantation, 16 mCi of ^{131}I was more effective than 16 mCi of ^{125}I in increasing the life span of rats bearing F98/hNIS gliomas, with ILS of 32.4 *versus* 14.7% (Table 1). There was no significant difference in the therapeutic effectiveness between the cocktail of $^{125}I/^{131}I$ (8 mCi each) and 16-mCi ^{131}I.

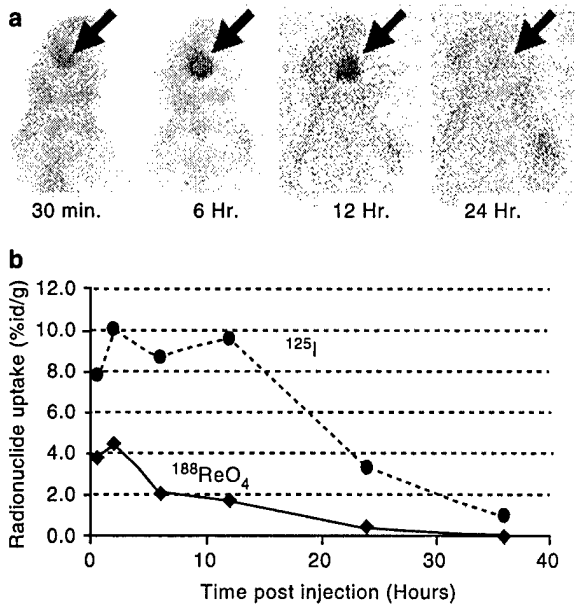

Figure 3 $^{188}ReO_4$ uptake in hNIS-transduced RG2 gliomas. (a) Serial $^{188}ReO_4$ planar imaging showed intense uptake in the brain tumor region (arrow) up to 12 h. Imaging was performed on rats implanted with 1×10^3 RG2/hNIS cells when the tumors approximated 3–6 mm in diameter. Changes in the imaging position of the rat account for the apparent variance in tumor size and location. N=4 per time point. (b) Time activity curves of $^{188}ReO_4$ (solid line) versus ^{125}I (dashed line) in RG2/hNIS gliomas showed higher uptake and longer retention time of ^{125}I. Rats implanted with 1×10^3 RG2/hNIS cells were coinjected with $^{188}ReO_4$ and ^{125}I when the tumors approximated 3–6 mm in diameter. After excision, tumors were weighed and counted for $^{188}ReO_4$ activity immediately. The same samples were counted for ^{125}I activity 1 week later. The data are presented as a percentage of injected dose (%ID/g) for each radionuclide after calibration with known standards. N=3 per time point.

The therapeutic effectiveness of ^{131}I may be affected by the number of fractions used to deliver the total radioactivity. Rats treated with 16 mCi of ^{131}I administered in three fractions had 32.4% ILS, while rats treated in two fractions had 45–55% ILS (Table 1). However, their difference in MST was not statistically significant (P=0.15, Student t-test).

$^{188}ReO_4$ is more efficient than ^{131}I treatment in prolonging the survival of rats bearing F98/hNIS gliomas

Among radioactive NIS substrates, β^- emissions released from $^{188}ReO_4$ are more potent than those of ^{131}I. We investigated the therapeutic efficacy of $^{188}ReO_4$ *versus* ^{131}I using the intracerebral F98/hNIS glioma animal model. Serial scintigraphy of F98/hNIS gliomas demonstrated detectable tumor $^{188}ReO_4$ uptake up to 12 h post radionuclide injection (Figure 3A). *Ex vivo* tissue gamma counting showed that maximal $^{188}ReO_4$ uptake in tumor occurred at 0.5 h post injection (Figure 3b), whereas $^{188}ReO_4$ uptake was minimal in adjacent normal brain tissue (data not shown). To compare tumor-absorbed dose delivered by $^{188}ReO_4$ *versus* ^{131}I at the same radioactivity dose, a dual-isotope, *ex vivo* biodistribution study with $^{188}ReO_4$ and ^{125}I was performed. ^{125}I was used in the study instead of ^{131}I, since both share the same pharmacokinetic properties and it is easier to quantify

the energy emitted by ^{125}I. As shown in Figure 3b, ^{125}I uptake was higher than $^{188}ReO_4$ uptake and the accumulated ^{125}I had a longer biological half-life than $^{188}ReO_4$ in RG2/hNIS gliomas (19.6 *versus* 6.3 h). Thus, the ratio of cumulative activity ($\tilde{A}$) for $^{188}ReO_4$ *versus* ^{131}I in RG2/hNIS gliomas was approximately 1:6, after modification of the time–activity curves of $^{188}ReO_4$ *versus* ^{125}I in tumor (Figure 3b) by the physical decay factors of ^{188}Re and ^{131}I, respectively. The ratio of nonpenetrating energy (Δnp) per transition for ^{188}Re *versus* ^{131}I is approximately 4:1 (1.66 *versus* 0.405 rad g/μCi h) when considering all the β^- particles, Auger and converting electrons as nonpenetrating emission.[25] By incorporating the factors of $\tilde{A}$ and Δnp, we concluded that the ratio of self-absorbed dose to tumors by $^{188}ReO_4$ *versus* ^{131}I was approximately 2:3, assuming that the nonpenetrating emission could be completely absorbed by the tumor.

The therapeutic efficacy of $^{188}ReO_4$ and ^{131}I in prolonging the survival of rats bearing intracerebral F98/hNIS gliomas was compared at equal radioactivity levels. Two batches of experiments were performed (Table 1). Rats treated with 8 mCi of $^{188}ReO_4$ had longer MSTs than rats treated with 8 mCi of ^{131}I. However, when the survival time of each rat was normalized to the mean of untreated controls by subtracting the MST of the associated untreated control group from the raw survival time, the difference was not statistically significant (Student's *t*-test, $P=0.09$).

Discussion

This study extends our initial finding of modest therapeutic effectiveness of ^{131}I in prolonging survival of rats bearing F98/hNIS intracerebral gliomas.[5] The finding that ^{131}I therapeutic effectiveness in F98/hNIS gliomas was dose-dependent suggests that dose escalation could further improve the efficacy of NIS-targeted ^{131}I therapy. The validation of NIS-targeted ^{131}I therapy in another animal model further supports our hypothesis that NIS-mediated radionuclide therapy may be useful to circumvent the problem of a narrow therapeutic window intrinsic to brain tumor radiotherapy. The observation that ^{131}I-treated gliomas had reduced percentages of NIS-expressing tumor cells, and that the extent of this reduction was more pronounced in rats with a longer survival time suggests a cytoreductive and/or a cytostatic effect of ^{131}I in hNIS-transduced tumor cells. Finally, the therapeutic effectiveness and efficiencies of ^{125}I and $^{188}ReO_4$ were demonstrated in rats bearing intracerebral hNIS-transduced gliomas. These findings suggest that NIS-mediated radionuclide therapy may be further improved by the selection of an appropriate radionuclide or combination of multiple radionuclides based on the nature of the tumor.

The effective doses required to achieve tumor control vary among different tumors. For patients with high-grade gliomas, it is recommended that a total dose of 50–60 Gy external radiation be delivered postoperatively.[26] For patients with metastatic thyroid cancer, ^{131}I therapy is believed to be effective when tumor absorbed dose is greater than 80 Gy.[27] Assuming a uniform distribution of radioactivity in a 1 mm diameter spherical F98/hNIS glioma in a rat treated with 16 mCi of ^{131}I 14 DPI, we estimated the absorbed dose to be 26 Gy (1.6 Gy/mCi), using the MIRD method.[28] Thus, a higher dose of ^{131}I may be warranted to further increase the survival time. A linear dose dependency of increased life span was observed without reaching a plateau (Table 1), suggesting that the dose of maximal therapeutic efficacy may not have been reached. In addition, little evidence of radiotoxicity was observed in rats given the maximum (16 mCi) dose of ^{131}I. While some of the rats did suffer temporary weight loss (1–2%), they recovered their weight in 3–6 days following ^{131}I treatment. It is likely that the weight loss was due to radioiodine-induced gastritis, a common side effect in patients treated with ^{131}I. Gross and microscopic post-mortem examination, however, showed no difference in the appearance of the gastric mucosa in treated rats.

The fact that the percentage of NIS-expressing cells was greatly reduced in ^{131}I-treated rats bearing RG2/hNIS gliomas, and that the degree of reduction correlated with the survival time of ^{131}I-treated rats suggest that ^{131}I had a cytoreduction effect on RG2/hNIS gliomas. By contrast, it is interesting to note that a reduction of NIS-expressing cells was not evident in ^{131}I-treated rats bearing F98/hNIS gliomas. Considering that rats bearing F98/hNIS gliomas had a prolonged survival by ^{131}I treatment, and that radioiodine uptake activity was diminished in ^{131}I-treated F98/hNIS gliomas (data not shown), it is most likely that ^{131}I had a cytostatic effect, rather than cytoreduction effect, on F98/hNIS gliomas.

The therapeutic effectiveness of ^{131}I administered 14 DPI (with undetectable tumor size) was greater than when administered 22 DPI (with tumor size of approximately 2 mm^3). This finding is in agreement with clinical observations that ^{131}I is more effective in treating microscopic, as opposed to macroscopic, metastatic thyroid cancer.[27,29,30] The maximal therapeutic effect of a radionuclide may occur when its emission spectrum matches the targeted tumor size.[31,32] The calculated optimal tumor diameter for ^{131}I treatment is 2.6–5.0 mm.[31] In our study, the tumor diameters at 14 and 22 DPI are less than 2.6 mm. De Jong *et al* reported that therapy appeared more effective at treating smaller tumors as opposed to larger tumors, when tumor size is outside the optimal size range for ^{90}Y-octreotide.[32]

^{131}I therapy appeared more effective in treating rats bearing F98/hNIS gliomas (45–55% ILS) than RG2/hNIS gliomas (26% ILS). This was surprising, not only because the intrinsic radiosensitivity of RG2 gliomas is reportedly greater than that of F98 tumors,[33] but also because our calculated tumor-absorbed doses of RG2/hNIS gliomas were higher than those of F98/hNIS gliomas in rats treated with the same ^{131}I activity. However, RG2/hNIS glioma had a higher proliferation rate *in vitro* and *in vivo*, as suggested by an MST of 24 days for untreated RG2/hNIS glioma-bearing rats compared to 35 days for untreated F98/hNIS gliomas-bearing rats in both group of rats following implantation of 1000 tumor cells. Consequently, the tumor sizes in rats bearing RG2/hNIS gliomas would be predicted to be larger than those in rats bearing F98/hNIS gliomas at 14 DPI, when ^{131}I was administered. Thus, while greater radiosensitivity and higher tumor absorbed dose should lead to a greater extent of cytoreduction, they do not necessarily translate to better tumor control. Indeed, our data showed that the reduction in NIS-expressing cells by ^{131}I therapy was

more pronounced in RG2/hNIS tumors than F98/hNIS tumors, yet rats bearing F98/hNIS gliomas had a higher %ILS. Thus, the efficacy of radionuclide therapy may be inadequate for tumors of high proliferative rate when viable tumor persists.

^{125}I emits ultra-short-ranged (generally less than 1 μm) Auger and Coster–Kronig electrons and produces high linear energy transfer (LET) cytotoxic effects, especially when ^{125}I is deposited in the proximity of the cell nucleus.[34–36] In small tumors, the majority of the ^{131}I β-decay energy deposition occurs outside the tumor, suggesting that ^{125}I may be more effective in such circumstances.[37] Conversely, in large tumors with an uneven distribution of radionuclide, ^{125}I may be inferior to ^{131}I, as Auger electrons would be ineffective against radionuclide-void tumor cells. Thus, a cocktail approach combining both Auger and β^- emission may have the benefit of multiple-emission ranges to span various tumor sizes and circumvent nonuniform absorbed dose distribution. Indeed, our studies have shown that 8 mCi each of $^{125}I/^{131}I$ is as effective as 16 mCi ^{131}I alone, despite a smaller tumor absorbed dose (15.4 Gy *versus* 25.6 Gy), assuming a tumor diameter of approximately 1 mm at 14 DPI.

Among NIS radioactive substrates, radioiodine is best suited to treat thyrocytes due to radioiodine retention from iodine organification. However, for cells lacking iodine organification, radionuclides such as $^{188}ReO_4$ with potent local emission may be superior. Compared to ^{131}I, $^{188}ReO_4$ has a higher nonpenetrating emission energy spectrum and a higher dose rate. Assuming that all the β-decay energy is absorbed in targeted tumors, Dadachova *et al* estimated that the ratio of tumor-absorbed dose by $^{188}ReO_4$ *versus* ^{131}I at the same level of radioactivity was about 4.5:1 using a murine xenograft model for breast cancer.[38] In contrast, our study showed a ratio of 2:3 using rats bearing NIS-transduced intracerebral glioma. In the xenografted breast cancer mouse model, comparable tumor uptake and retention time were observed resulting in slightly higher cumulative activity of $^{188}ReO_4$ than that of ^{125}I.[38] In contrast, rats bearing intracerebral RG2/hNIS gliomas had a six-fold lower cumulative activity of $^{188}ReO_4$ than ^{131}I, due to lower tumor uptake and shorter retention time. The lower $^{188}ReO_4$ uptake compared to radioiodine in intracerebral NIS-transduced gliomas may be due to its larger size or its metal nature, and therefore, decreased permeability to the BBB. Indeed, lower $^{188}ReO_4$ uptake compared to ^{125}I was also observed in normal brain tissues (data not shown). The shorter retention time of $^{188}ReO_4$ than ^{125}I in NIS-transduced gliomas might be the result of a difference in their efflux rate. Alternatively, a faster clearance of $^{188}ReO_4$ than ^{125}I from blood circulation may also contribute to a shorter retention time of $^{188}ReO_4$ in NIS-transduced gliomas.[39,40] The slower clearance of ^{125}I from blood circulation is anticipated by the large iodide pool *in vivo* that is contributed by the thyroid gland reservoir and entero-recirculation.[41]

While ^{188}Re has been investigated for various clinical applications, such as endovascular brachytherapy or labeling various compounds to treat cancer and to palliate bone pain,[42,43] this is the first report to examine the therapeutic effectiveness of $^{188}ReO_4$ for NIS-expressing tumors. Assuming the tumor diameter was approximately about 1 mm at 14 DPI, the tumor-absorbed dose for rats carrying F98/hNIS gliomas treated with 8 mCi of $^{188}ReO_4$ was estimated to be 2 Gy with 51.2–78.1% ILS achieved. In comparison, 12 Gy of tumor-absorbed dose was delivered to similar rats by 8 mCi of ^{131}I with 35.8–40.3% ILS achieved. Thus, $^{188}ReO_4$ appeared to be more efficient than ^{131}I in prolonging the survival of rats bearing F98/hNIS gliomas. This is likely explained by the greater energy release in a short time interval by ^{188}Re compared to ^{131}I, 1096 *versus* 24 keV/day, respectively.[44] Other benefits of using $^{188}ReO_4$, instead of ^{131}I, to treat nonthyroidal malignancies include the potential for less damage to the thyroid gland given the lack of $^{188}ReO_4$ organification,[38] and superior gamma scintigraphy qualities. Recently, NIS-mediated uptake of ^{211}At, an α emitter with high LET, was demonstrated.[45,46] Thus, ^{211}At may potentially be useful for NIS-targeted radionuclide therapy.

Materials and methods

Establishment of rat models bearing intracerebral human NIS expressing F98 or RG2 gliomas

The protocol to establish a rat model bearing human NIS (hNIS) expressing F98 gliomas was described previously.[5] A DNA construct containing full-length hNIS cDNA driven by the Moloney murine leukemia virus long terminal repeat (LTR) promoter and a selection marker Neo^r driven by SV40 promoter (referred to as L-hNIS-SN) was created and transfected into PA317 retroviral packaging cells. PA317 cells carrying L-hNIS-SN were selected by geneticin (G418) treatment (Gibco BRL, Grand Island, NY, USA), and stable clones were selected that produce the recombinant retrovirus carrying hNIS. As a control, we produced a recombinant retrovirus carrying empty vector (L-X-SN). F98 or RG2 rat glioma cells were infected with recombinant retrovirus carrying L-hNIS-SN and selected by G418. Clonal cell lines with stable NIS expression (referred to as F98/hNIS and RG2/hNIS, respectively) were isolated and expanded. Colonies showing the highest *in vitro* ^{125}I uptake (~40 times in F98/hNIS and ~120 times in RG2/hNIS, as compared to the non-NIS transduced controls) were used for further experiments. The control (F98/LXSN or RG2/LXSN) indicated respective glioma cells carrying the empty vector, L-X-SN, which was generated in a similar procedure.

Male Fisher rats (Harlan Inc., Indianapolis, IN, USA) weighing ~200 g were stereotactically implanted with tumor cells, as described elsewhere.[47,48] Following induction of anesthesia with an intraperitoneal (i.p.) dose of 20 mg ketamine/120 mg xylazine mixture per kilogram of body weight (Fort Dodge, Fort Dodge, IA, USA) in 0.2 ml volume, 1000 tumor cells in 10 l of serum-free DMEM containing 1.4% agarose were injected over 10–15 s into the right hemisphere using a stereotactic instrument. At 1 week prior to the radionuclide therapy, imaging studies, or radionuclide biodistribution studies, rats were placed on a 1 ppm thyroxin (T4)-supplemented diet (Harlan Teklad, Madison, WI, USA).[5] All experimental procedures received approval from the Institutional Laboratory Animal Care and Use Committee of The Ohio State University.

Scintigraphic studies of the biological retention time of ^{123}I or $^{188}ReO_4$ in NIS-transduced tumor

Serial ^{123}I or $^{188}ReO_4$ scintigraphies were performed 30 min, 4–6 h, 12–14 h, and 24–26 h post ^{123}I or $^{188}ReO_4$ i.p. injection to determine the biological retention time of the respective radioisotope in intracerebral tumors. Tumor-bearing rats were imaged under anesthesia by i.p. injection of the ketamine/xylazine mixture. A dual head gamma camera (Picker Prism 2000XP Baseline V8.5A, gantry-fixed, PCD- and SPECT-capable, Marconi Medical Systems, Cleveland, OH, USA) equipped with a pinhole collimator and a low-energy ultra-high-resolution parallel hole collimator (LEUHR), respectively, on each head of the gamma camera was used for imaging acquisition so that a focal brain view and a whole body view were obtained simultaneously. ^{123}I was purchased from MDS Nordion Company (Toronto, Canada) and $^{188}ReO_4$ was eluted from a ^{188}Tungsten/^{188}Rhenium generator purchased from Oak Ridge National Lab (Oakridge, TN, USA). Tumor-bearing rats were injected i.p. with 1 mCi ^{123}I in 0.5 ml volume or 2.5 mCi $^{188}ReO_4$ in 0.5 ml and placed in prone and supine positions so that conjugated views (ie vertex and ventral) could be acquired at the indicated time postinjection. The total injected dose was calculated by subtracting the post-injected syringe counts from the preinjected syringe counts. For subsequent calibration of tumor radioactivity, a 1-ml syringe containing a known amount of the respective radionuclide was included as a standard dose and underwent the same tumor imaging procedure. The acquisition time for each time point was 5 min. Regions of interest (ROI) were drawn over the tumor and shoulder region (as a background) in two views (vertex and then ventral) of pinhole images for each different time point. After subtraction of background counts, the geometric means of the counts rates (CPM) for tumor ROI in each view were determined. The background-corrected count rates of tumor regions were calibrated by standard count rates at each time point and calculated as percentage of injected dose (%ID).

To determine the average uptake value of tumor (%ID per gram of tumor, ie %ID/g), tumor-bearing rats were first intravenously (i.v.) injected with 2% Evans Blue (Sigma, St Louis, MO, USA) in 1 ml normal saline to stain the BBB breakdown site, localizing the brain tumor region. The tumor weight was determined by weighing the Evans blue-stained tumor excised from the corresponding rat brain after imaging was completed. The tumor radionuclide uptake was calculated and expressed as %ID/g. Biological half-life ($T_{1/2}$) of radionuclide in tumor was estimated based on the time activity curve (TAC) generated by plotting the tumor ROI count rates or %ID/g *versus* time.

Ex vivo measurement of in vivo ^{125}I uptake in tumor and other tissues

^{125}I biodistribution studies were performed using groups of tumor-bearing rats injected i.p. with carrier-free ^{125}I (Amersham Pharmacia Biotech, Piscataway, NJ, USA) at 0.15 μCi per gram of body weight in 0.5 ml of normal saline. Total administered radioactivity counts were calculated by subtracting the radioactivity of the post-injected syringe from that of the preinjected one measured by a γ-counter (Packard, GMI, Inc., MN, USA) for each animal injection. Prior to the euthanization of animals, 2% Evans Blue in 1 ml normal saline was injected intravenously to localize the brain tumor region. Groups of rats (three rats per group) were killed by CO_2 asphyxia at the indicated time post ^{125}I injection, and 1-ml blood, thyroid gland, stomach, salivary gland, lung, liver and spleen, as well as the brain were collected. Next, the brain was cut into 2-mm coronal sections with a rat brain slicer (Zivic-Miller Laboratories, Inc., Allison Park, PA, USA). From each section, the Evans blue-stained tissue and a piece of unstained brain tissue were excised, weighed, and measured for their radioactivity by a γ-counter. After normalization for total administered radioactivity, the average uptake value of radioiodine in tissues of interest was determined as %ID/g.

Dual isotope (^{125}I versus $^{188}ReO_4$) dosimetric study by ex vivo tissue counting

Simultaneous administration of ^{125}I and $^{188}ReO_4$ into NIS-transduced glioma-bearing rats was performed in order to compare the biodistribution and retention time of respective radioisotopes as previously described.[38] A mixture of 0.15 μCi ^{125}I and 2.5 μCi $^{188}ReO_4$ per gram of body weight in 0.5 ml normal saline was injected i.p. to rats bearing intracerebral tumors about 3–6 mm in diameter. Evans blue solution was injected i.v. prior to euthanization at 30 min, 2 h, 6 h, 12 h, and 24 h post radionuclide injection, animals ($N \geq 3$ at each time point) were euthanized by CO_2-induced asphyxia. Evans blue-stained brain tumors, as well as other tissues, were collected and counted for ^{188}Re radioactivity using its γ energy window (155 ± 20 KeV). After 1 week, when ^{188}Re radioactivity had decayed, the tissues were counted for ^{125}I radioactivity in its γ energy window (35 ± 10 KeV). The total administered radioactivity for each radionuclide was measured in counts by subtracting the radioactivity of the postinjected syringe from that of the corresponding preinjected one for each animal in the study. The average uptake value (%ID/g) of respective radionuclides in tumors and other tissues at different time points was determined. TACs of ^{125}I *versus* $^{188}ReO_4$ in tissues of interest was generated by plotting the average uptake value *versus* time.

^{131}I, ^{125}I, and $^{188}ReO_4$ treatment of glioma-bearing rats

The dose, regimen, isotope, and sample number in different experimental animal batches are summarized in Table 1. To investigate the therapeutic effectiveness of ^{125}I, we compared the prolonged survival of rats bearing F98/hNIS gliomas treated with 16 mCi of ^{131}I (N=6), 16 mCi of ^{125}I (N=6), or 8 mCi of each (N=6) with untreated groups (N=7). The total dose was divided into three fractions.

One experimental study was performed to compare the therapeutic effectiveness of 16 mCi of ^{131}I treatment in rats bearing F98/hNIS gliomas on DPI 14 (N=8) *versus* 22 (N=8), and an untreated group (N=3) was included. The regimen was modified into two fractions 12 h apart and was used through all of the following experiments. Dose dependency of ^{131}I treatment was analyzed by performing an experiment with 16 mCi (N=7) *versus* 4 mCi (N=6) treatments *versus* untreated (N=6) rats bearing F98/hNIS gliomas, in addition to the data

acquired from other batches of experiments that used different doses (8 and 5.6 mCi).

To compare the therapeutic effectiveness of $^{188}ReO_4$ *versus* ^{131}I in prolonging the survival of F98/hNIS glioma-bearing rats, experimental groups with 8 mCi $^{188}ReO_4$ (N=8), and 8 mCi ^{131}I (N=7) treatments, along with an untreated control animals (N=6), were studied to compare the survival of animals. Due to the limited amount of $^{188}ReO_4$ production from the ^{188}Tungsten/^{188}Rhenium generator at one time, the treatment experiment was divided into two batches.

RG2 glioma-bearing rats were also included to investigate the resulting survival times by strategies of NIS gene transfer alone (N=7), LXSN vector transfer (N=7) alone, 16-mCi ^{131}I treatment of nontransduced tumors (N=7), or NIS gene transfer followed by 16-mCi ^{131}I treatment (N=10) in comparison with the control group, that is wild-type RG2 (N=5).

The survival time of each animal was determined as previously described.[5] Rats were euthanized when they displayed moribund signs, which consisted of sustained weight loss, ataxia, and periorbital hemorrhage. Survival times were determined as the day of tumor implantation to the day of euthanization plus 1 day. The observers were not blinded when killing the rats. All tumor-bearing animals were grossly examined for any abnormality of their viscera in necropsy. The intracerebral tumors were confirmed by routine histopathological examination of hematoxylin and eosin-stained tissues sections, unless they were used for *ex vivo* measurement of ^{125}I uptake.

Anti-hNIS immunohistochemical (IHC) staining

IHC staining was performed as previously described with some modifications. Briefly, tissue sections were incubated with hNIS polyclonal antibody #331 (1:1,000 dilution) at room temperature for 1 h, and then incubated with biotinylated goat anti-rabbit IgG (1:200 dilution, Vector Lab. Inc., Burlingame, CA, USA) for 20 min. To semiquantify the hNIS IHC signal, the following 0 to 4+ system was used to estimate the percentage of NIS-expressing tumor cells: 0+0, 1+25, 2+50, 3+75, and 4+100%.

Statistics

The average uptake values of radionuclides in tissues of interest were expressed as mean$\pm$s.d. Survival time among different experimental groups was also expressed as mean$\pm$s.d. and then MSTs were compared using a two-tailed, unpaired t-test with assumption of unequal variance. When multiple comparisons were made, the difference of MST for one indicated group from the others was determined by one-way ANOVA with Dunnett's test. The %ILS was determined as the ratio of the difference between the MST of experimental and untreated control groups and the MST of untreated control group multiplied by 100%. Regression analysis was performed to test the correlation between therapeutic ^{131}I dose and resulting %ILS and between hNIS IHC grading and survival time. A P-value <0.05 was considered statistically significant. All statistical analyses were performed using SAS JMP Version 4 (SAS Institute, Cary, NC, USA).

Acknowledgements

We are indebted to our Nuclear Medicine colleagues of The Ohio State University Hospital, including Ms Bonnie Williams, Mr Cowan Edwards, Mr Aaron Haynam, and Ms Mary Morgan for their preparation of radionuclides and providing gamma camera assistance. We also thank Dr FF Russ Knapp at the Oak Ridge National Lab for his consultation regarding use of the ^{188}Tungsten/^{188}Rhenium generator. This work was partly supported by DOD Prostate Cancer Research Program DAMD 17-02-0119 (to SMJ), and the statistical analyses were supported by NIH Grant #MO1 RR00034 (to HNN via OSU GCRC).

References

1 Dai G, Levy O, Carrasco N. Cloning and characterization of the thyroid iodide transporter. *Nature* 1996; **379**: 458–460.
2 Smanik PA *et al*. Cloning of the human sodium lodide symporter. *Biochem Biophys Res Commun* 1996; **226**: 339–345.
3 Shimura H *et al*. Iodide uptake and experimental ^{131}I therapy in transplanted undifferentiated thyroid cancer cells expressing the Na+/I− symporter gene. *Endocrinology* 1997; **138**: 4493–4496.
4 Mandell RB, Mandell LZ, Link Jr CJ. Radioisotope concentrator gene therapy using the sodium/iodide symporter gene. *Cancer Res* 1999; **59**: 661–668.
5 Cho JY *et al*. *In vivo* imaging and radioiodine therapy following sodium iodide symporter gene transfer in animal model of intracerebral gliomas. *Gene Therapy* 2002; **9**: 1139–1145.
6 La Perle KM *et al*. *In vivo* expression and function of the sodium iodide symporter following gene transfer in the MATLyLu rat model of metastatic prostate cancer. *Prostate* 2002; **50**: 170–178.
7 Boland A *et al*. Adenovirus-mediated transfer of the thyroid sodium/iodide symporter gene into tumors for a targeted radiotherapy. *Cancer Res* 2000; **60**: 3484–3492.
8 Nakamoto Y *et al*. Establishment and characterization of a breast cancer cell line expressing Na+/I- symporters for radioiodide concentrator gene therapy. *J Nucl Med* 2000; **41**: 1898–1904.
9 Haberkorn U *et al*. Transfer of the human NaI symporter gene enhances iodide uptake in hepatoma cells. *J Nucl Med* 2001; **42**: 317–325.
10 Spitzweg C *et al*. Prostate-specific antigen (PSA) promoter-driven androgen-inducible expression of sodium iodide symporter in prostate cancer cell lines. *Cancer Res* 1999; **59**: 2136–2141.
11 Carlin S *et al*. Experimental targeted radioiodide therapy following transfection of the sodium iodide symporter gene: effect on clonogenicity in both two- and three-dimensional models. *Cancer Gene Ther* 2000; **7**: 1529–1536.
12 Spitzweg C *et al*. *In vivo* sodium iodide symporter gene therapy of prostate cancer. *Gene Therapy* 2001; **8**: 1524–1531.
13 Prados MD, Levin V. Biology and treatment of malignant glioma. *Semin Oncol* 2000; **27**: 1–10.
14 Brandes AA, Rigon A, Monfardini S. Radiotherapy of the brain in elderly patients. *Contra Eur J Cancer* 2000; **36**: 447–451; discussion 451–442.
15 Grau JJ, Verger E. Radiotherapy of the brain in elderly patients. *Pro Eur J Cancer* 2000; **36**: 443–447.
16 Wheldon TE. Radiation physics and genetic targeting: new directions for radiotherapy. The Douglas Lea Lecture 1999. *Phys Med Biol* 2000; **45**: R77–R95.
17 McDermott MW, Gutin PH, Larson DA, Sneed PK. Interstitial brachytherapy. *Neurosurg Clin N Am* 1990; **1**: 801–824.
18 Mann BD *et al*. Imaging of human tumor xenografts in nude mice with radiolabeled monoclonal antibodies. Limitations of

specificity due to nonspecific uptake of antibody. *Cancer* 1984; **54**: 1318–1327.
19 Goodwin DA. Pharmacokinetics and antibodies. *J Nucl Med* 1987; **28**: 1358–1362.
20 Goodwin DA *et al*. Pre-targeted immunoscintigraphy of murine tumors with indium-111-labeled bifunctional haptens. *J Nucl Med* 1988; **29**: 226–234.
21 Riva P *et al*. Local application of radiolabeled monoclonal antibodies in the treatment of high grade malignant gliomas: a six-year clinical experience. *Cancer* 1997; **80**: 2733–2742.
22 Riva P *et al*. Loco-regional radioimmunotherapy of high-grade malignant gliomas using specific monoclonal antibodies labeled with 90Y: a phase I study. *Clin Cancer Res* 1999; **5**: 3275s–3280s.
23 Riva P *et al*. ^{131}I radioconjugated antibodies for the locoregional radioimmunotherapy of high-grade malignant glioma – phase I and II study. *Acta Oncol* 1999; **38**: 351–359.
24 Riva P *et al*. Role of nuclear medicine in the treatment of malignant gliomas: the locoregional radioimmunotherapy approach. *Eur J Nucl Med* 2000; **27**: 601–609.
25 Weber DA. *MIRD: Radionuclide Data and Decay Schemes*. The Society of Nuclear Medicine: New York, 1989.
26 Laperriere N, Zuraw L, Cairncross G. Radiotherapy for newly diagnosed malignant glioma in adults: a systematic review. *Radiother Oncol* 2002; **64**: 259–273.
27 Maxon HR, Thomas SR, Samaratunga RC. Dosimetric considerations in the radioiodine treatment of macrometastases and micrometastases from differentiated thyroid cancer. *Thyroid* 1997; **7**: 183–187.
28 Loevinger R, Budinger TF, Watson EE. *MIRD Primer For Absorbed Dose Calculation*. The Society of Nuclear Medicine: New York, NY, 1991.
29 Casara D *et al*. Different features of pulmonary metastases in differentiated thyroid cancer: natural history and multivariate statistical analysis of prognostic variables. *J Nucl Med* 1993; **34**: 1626–1631.
30 Sherman SI. The management of metastatic differentiated thyroid carcinoma. *Rev Endocr Metab Disord* 2000; **1**: 165–171.
31 O'Donoghue JA, Bardies M, Wheldon TE. Relationships between tumor size and curability for uniformly targeted therapy with beta-emitting radionuclides. *J Nucl Med* 1995; **36**: 1902–1909.
32 de Jong M *et al*. Tumor response after [(90)Y-DOTA(0),Tyr(3)]octreotide radionuclide therapy in a transplantable rat tumor model is dependent on tumor size. *J Nucl Med* 2001; **42**: 1841–1846.
33 Knedlitschek G, Anderer U, Weibezahn KF, Dertinger H. Radioresistance of rat glioma cell lines cultured as multicellular spheroids. Correlation with electrical cell-to-cell-coupling. *Strahlenther Onkol* 1990; **166**: 164–167.
34 Bloomer WD, McLaughlin WH, Adelstein SJ, Wolf AP. Therapeutic applications of Auger and alpha emitting radionuclides. *Strahlentherapie* 1984; **160**: 755–757.
35 O'Donoghue JA, Wheldon TE. Targeted radiotherapy using Auger electron emitters. *Phys Med Biol* 1996; **41**: 1973–1992.
36 O'Donoghue JA. Strategies for selective targeting of Auger electron emitters to tumor cells. *J Nucl Med* 1996; **37**: 3S–6S.
37 Cunningham SH *et al*. Toxicity to neuroblastoma cells and spheroids of benzylguanidine conjugated to radionuclides with short-range emissions. *Br J Cancer* 1998; **77**: 2061–2068.
38 Dadachova E, Bouzahzah B, Zuckier LS, Pestell RG. Rhenium-188 as an alternative to Iodine-131 for treatment of breast tumors expressing the sodium/iodide symporter (NIS). *Nucl Med Biol* 2002; **29**: 13–18.
39 Knapp Jr FF *et al*. Endovascular beta irradiation for prevention of restenosis using solution radioisotopes: pharmacologic and dosimetric properties of rhenium-188 compounds. *Cardiovasc Radiat Med* 1999; **1**: 86–97.
40 Lin WY *et al*. A comprehensive study on the blockage of thyroid and gastric uptakes of ^{188}Re-perrhenate in endovascular irradiation using liquid-filled balloon to prevent restenosis. *Nucl Med Biol* 2000; **27**: 83–87.
41 Josefsson M, Grunditz T, Ohlsson T, Ekblad E. Sodium/iodide-symporter: distribution in different mammals and role in entero-thyroid circulation of iodide. *Acta Physiol Scand* 2002; **175**: 129–137.
42 Knapp Jr FF. Rhenium-188 – a generator-derived radioisotope for cancer therapy. *Cancer Biother Radiopharm* 1998; **13**: 337–349.
43 Knapp Jr FF *et al*. Reactor-produced radioisotopes from ORNL for bone pain palliation. *Appl Radiat Isot* 1998; **49**: 309–315.
44 O'Donoghue J. Dosimetric Principles of Targeted Radiotherapy. In: Abrams PG FA (ed). *Radioimmunotherapy of Cancer*. Marcel Dekker: New York, 2000, pp 1–21.
45 Petrich T *et al*. Establishment of radioactive astatine and iodine uptake in cancer cell lines expressing the human sodium/iodide symporter. *Eur J Nucl Med Mol Imaging* 2002; **29**: 842–854.
46 Carlin S, Mairs RJ, Welsh P, Zalutsky MR. Sodium-iodide symporter (NIS)-mediated accumulation of [(211)At]astatide in NIS-transfected human cancer cells. *Nucl Med Biol* 2002; **29**: 729–739.
47 Kobayashi N, Allen N, Clendenon NR, Ko LW. An improved rat brain-tumor model. *J Neurosurg* 1980; **53**: 808–815.
48 Clendenon NR *et al*. Enhanced survival in a rat glioma model following BNCT. *Strahlenther Onkol* 1989; **165**: 222–225.

Appendix 3

Cancer Gene Therapy (2003) 00, 00–00

www.nature.com/cgt

Imaging of metastatic pulmonary tumors following NIS gene transfer using single photon emission computed tomography

Derek K Marsee,[1] Daniel HY Shen,[2,3] Lawrence R MacDonald,[4] Douangsone D Vadysirisack,[2] Xiaoqin Lin,[2] George Hinkle,[5] Richard T Kloos,[3,6] and Sissy M Jhiang[2,6]

[1]Medical Scientist Program, College of Medicine and Public Health, The Ohio State University, Columbus, Ohio, USA; [2]Department of Physiology and Cell Biology, College of Medicine and Public Health, The Ohio State University, Columbus, Ohio, USA; [3]Department of Nuclear Medicine, Tri-Service General Hospital, National Defense Medical Center, Taipei, ROC; [4]Gamma Medica, Division of Photon Imaging, Inc., Northridge, California 91324, USA; [5]Department of Radiology, College of Medicine and Public Health, The Ohio State University, Columbus, Ohio, USA; and [6]Department of Internal Medicine, College of Medicine and Public Health, The Ohio State University, Columbus, Ohio, USA.

The Na^+/I^- symporter (NIS) is a membrane glycoprotein that facilitates the uptake of iodine into thyroid follicular cells. Recently, we and others have demonstrated the feasibility of imaging subcutaneous xenografts expressing exogenous NIS, suggesting that NIS may serve as an imaging reporter gene to monitor vector delivery and therapeutic gene expression. In this study, we established NIS-expressing pulmonary tumors in nude mice to investigate the minimal tumor size required for *in vivo* detection of pulmonary tumors by single photon emission computed tomography (SPECT) with pinhole collimation. In order to define the anatomic location of NIS-expressing tumor nodules detectable by SPECT, we performed simultaneous, dual-isotope imaging. We injected 1 mCi ^{99m}Tc-MAA via tail vein to image pulmonary perfusion and injected 1 mCi $Na^{125}I$ intraperitoneally to image NIS-expressing tumors. Fused images showed that ^{99m}Tc-MAA perfusion defects correlated with NIS-mediated ^{125}I uptake. Post-mortem analysis revealed that tumors 3 mm in diameter could be detected by SPECT with pinhole collimation. These studies demonstrate the feasibility of SPECT to detect pulmonary tumors expressing exogenous NIS in mice.
Cancer Gene Therapy (2003) **0,** 000–000. doi:10.1038/sj.cgt.7700661

Keywords: sodium iodide symporter; SPECT; nuclear imaging; gene therapy

The sodium/iodide symporter (NIS) is an intrinsic membrane glycoprotein with 13 putative transmembrane domains. Electrophysiologic studies have shown that NIS functions by cotransporting one I^- ion with two Na^+ ions into cells.[1] In addition, other selected anions (e.g. ReO_4 and TcO_4) are readily transported by NIS. Consequently, NIS-expressing cells will uptake radionuclides such as ^{131}I, ^{123}I, ^{125}I, ^{99m}Tc, and ^{188}Re, resulting in their intracellular accumulation. In tissues where NIS protein is endogenously expressed, including the thyroid,[2–4] stomach,[5,6] salivary gland,[7–9] and lactating breast,[10,11] the accumulation of these radionuclides can be detected *in vivo* by nuclear imaging. Use of these radioisotopes has long been essential to the diagnosis and treatment of thyroid diseases,[12] and numerous studies have been conducted to investigate the use of NIS-mediated radionuclide accumulation in the diagnosis and treatment of nonthyroid malignancies.

Received May 28, 2003.
Correspondence: Dr SM Jhiang, Department of Physiology and Cell Biology, The Ohio State University, 304 Hamilton Hall, 1645 Neil Avenue, Columbus, OH 43210, USA. E-mail: jhiang.1@osu.edu

Since the cloning of NIS in 1996,[3,4] interest in the use of NIS as an imaging reporter gene has risen for several reasons. First, NIS is not a foreign gene; hence, it is nonimmunogenic. Second, the tissue expression profile of endogenous NIS protein is limited; as a result, imaging of exogenous NIS function can be performed in a wide variety of tissues due to limited background interference. Third, NIS mediates the uptake of radioisotopes and simple radiopharmaceuticals; therefore, complicated synthesis and labeling of substrate molecules is not required for imaging. Fourth, the radionuclides employed are specific to NIS-expressing cells, which reduces unwanted background signal. Fifth, both NIS-mediated radionuclide uptake and background clearing are rapid, which makes imaging feasible. In summary, NIS and its radionuclides possess qualities favorable for an imaging reporter gene toward the monitoring and optimization of gene delivery and expression.

The first imaging trial in tumors expressing exogenous NIS was performed using autoradiography of rats carrying NIS-transfected FRTL-Tc cells, a transformed rat thyroid cell line that has lost its endogenous NIS expression.[13] Subsequently, *in vivo* planar scintigraphy

Gml : Ver 6.0
Template: Ver 1.0

Journal: CGT ☐ Disk used Despatch Date: 28/10/2003
Article : npg_CGT_7700661 Pages: 7 Col figs. 2 – 5 KGU/Suja

has been performed on NIS-transduced A375 human melanoma cells,[14] LNCaP human prostate carcinoma cells,[15] MH3924 hepatoma cells,[16] SiHa human cervical carcinoma cells,[17] MATLyLu (MLL) rat prostate cancer cells,[18] F98 rat glioma cells,[19] and ARH-77 multiple myeloma cells.[20] A variety of delivery methods, including adenoviral[11,17] and retroviral[16,18] transduction, have been used to transfer exogenous NIS to these nonthyroid cell lines, demonstrating the broad range of cell types and delivery methods that can be employed in exogenous NIS gene delivery.

Whereas the majority of these studies exploring NIS as an imaging reporter gene have used planar scintigraphy, ^{124}I positron emission tomography (PET) has also been used recently to detect xenografts expressing exogenous NIS in mice.[21] To date, no studies have examined the use of single photon emission computed tomography (SPECT) to image exogenous NIS expression. Unlike PET, SPECT is more readily available and does not require positron emitting radionuclides.[22] In this study, we examine the ability of SPECT to detect NIS-expressing pulmonary tumor nodules in nude mice. We demonstrate that multiple, discrete pulmonary NIS-expressing tumors can be detected in nude mice, using ^{99m}Tc and ^{125}I SPECT. Post-mortem analysis combined with dual-isotope SPECT showed that tumors as small as 3 mm in diameter can be detected.

Materials and methods

Cell culture and in vivo *tumor formation*

The anaplastic rat prostate tumor cell line MLL were grown in RPMI media supplemented with 10% FBS, 2 mM L-glutamine, 10 mg/ml insulin, 5.5 mg/ml transferrin, 6.7 μg/ml sodium selenite, and 10 U penicillin/streptomycin. The generation of MLL/NIS cells has been previously described.[18] NIS expression was maintained in these cells by the presence of 400 mg/ml G-418.

Male 2-month-old BALB/c nu/nu mice (Taconic; Germantown, NY) were housed in a sterile environment with food and water *ad libitum*. Pulmonary tumors were generated by tail vein injection of cells in a volume of 0.25 ml PBS.

Flow cytometry analysis of NIS expression

MLL/NIS cells (1×10^6) were incubated with VJ2 α-NIS mAb[23] diluted 1:50 in FACS buffer (3% FBS, 0.02%. NaN_3 in PBS) at room temperature for 30 minutes. The cells were then washed once with FACS buffer and incubated with FITC-conjugated α-mouse IgG (Sigma) diluted 1:100 in FACS buffer on ice for 30 minutes. The cells were washed again in FACS buffer and resuspended in fixative buffer (1% paraformaldehyde in PBS). Fluorescence was analyzed in 5,000 cells, using Cell Quest software (Becton Dickinson). Secondary antibody alone was used as a negative control. The percentage of NIS-expressing cells was determined by gating the right side of the negative control population at 0.5%.

Immunohistochemical staining of pulmonary tumors

Formalin-fixed lung tissues were dehydrated and embedded in paraffin blocks. Sections were cut at 10 μm, deparaffinized, and rehydrated. After blocking in 3% H_2O_2 for 5 minutes, the sections were rinsed in distilled water and placed in a steamer containing citric acid buffer (pH 5.93) for 60 minutes for antigen retrieval. Sections were incubated with polyclonal α-NIS #331[7] (1:500) in TBS + 1% BSA for 1 hour in a humidified chamber at room temperature. The sections were rinsed in TBS and incubated with HRP-conjugated α-rabbit IgG (Cell Signaling) for 1 hour in a humidified chamber at room temperature. The slides were rinsed again in TBS and incubated with chromagen substrate (Dako) for 5 minutes in a dark chamber. After rinsing with TBS, the slides were counterstained with hematoxylin.

Radioactive iodine uptake assay

MLL cells stably infected with retrovirus expressing either NIS or vector alone were seeded (5×10^4 cells/well) in 24-well plates. After 1 day, the cells were incubated with media containing 2.0 μCi $Na^{125}I$ and 5 mM cold NaI for 30 minutes at 37°C in 5% CO_2. Cells were washed twice with ice-cold HBSS and lysed with cold 95% ethanol. The cell lysate was collected and counted for ^{125}I activity. Data are presented as cpm/1×10^5 cells.

^{99m}Tc SPECT studies of MLL/NIS lung tumors

We injected nude mice with 2×10^3, 1×10^4, or 1×10^5 MLL/NIS or vector-only MLL (MLL/LXSN) cells via tail vein and performed ^{99m}Tc SPECT every 3–5 days, post-tumor injection. All SPECT studies were performed using an A-SPECT™ system provided by Gamma Medica, Inc. (Northridge, CA). Animals were given an intraperitoneal (i.p.) injection of 1 mCi $Na^{99m}TcO_4$ and after 20 minutes were anesthetized using isofluorane inhalation. The animals were secured in the rotating animal holder and a nose cone was used to ensure that the animal remained sedated for the duration of SPECT acquisition. SPECT acquisition was performed using a pinhole collimator with an aperture of 1.0 mm and a 2.4 cm radius of rotation. In all, 64 projections at 60 seconds/image were collected, with a duration of 60 seconds/image. The energy window for ^{99m}Tc was set at 141 keV ±10%. Postreconstruction filtering was performed using the Butterworth, band-pass method.

Dual-isotope ^{99m}Tc-MAA and ^{125}I SPECT studies of MLL/NIS lung tumors

At 2 hours before image acquisition, animals were injected i.p. with 1 mCi $Na^{125}I$. At 30 minutes before image acquisition, the animals were injected via tail vein with 1 mCi ^{99m}Tc-MAA (DraxImage) in a volume of 0.25 ml. The animals were anesthetized with isofluorane and SPECT imaged as described above. We performed

simultaneous image acquisition, using separate energy windows for ^{125}I (35 keV $\pm$10%) and ^{99m}Tc (141 keV $\pm$10%). Scattering contamination of ^{99m}Tc into the ^{125}I window was nonexistent or negligible, due to the small size of the mouse and the relatively large difference in energies between the ^{99m}Tc and ^{125}I γrays. Image fusion was performed using IDL software (Research Systems, Inc.).

Results

NIS-transduced MLL cells can uptake radioiodine in vitro

Parental MLL cells do not express the endogenous NIS gene and are unable to uptake radioiodine (data not shown). For our studies, we utilized a stable MLL cell line that had been infected with replication-defective retrovirus expressing NIS (MLL/NIS).[18] Flow cytometry analysis using nonpermeabilized MLL/NIS cells showed that surface NIS expression was detectable in 85% of cells (Fig 1, top panel). Analysis of NIS function showed that MLL/NIS cells had a 25-fold increase in RAIU, compared to vector-only MLL cells (Fig. 1, bottom panel).

Injection of higher numbers of MLL/NIS cells correlated with an earlier date of tumor nodule detection using ^{99m}Tc SPECT

Immunohistochemical staining of MLL/NIS pulmonary tumors in nude mice demonstrated NIS membrane staining in tumor cells, with no staining in the pulmonary parenchema (Fig 2, lower panel). By contrast, NIS staining was not detectable in any of the MLL/LXSN cells, which carry the retroviral vector lacking NIS (Fig 2, upper panel). The majority of MLL/NIS tumors were found on the surface of the lung, although occasional tumors were also seen surrounding blood vessels (data not shown). To screen for tumors by SPECT, we injected nude mice with 2×10^3, 1×10^4, or 1×10^5 MLL/NIS or vector-only MLL (MLL/LXSN) cells via tail vein and performed ^{99m}Tc SPECT every 3–5 days, post-tumor injection. Pulmonary tumor nodules were readily detected by SPECT in mice injected via tail vein with 2×10^3, 1×10^4, and 1×10^5 cells by 20, 17, and 14 days postimplantation, respectively (Table 1), after which animals were killed. We counted the number of tumors on the pulmonary surface and measured their maximal diameters (Table 1). Whereas the number of tumors that developed after injection with either 2×10^3 or 1×10^4 cells varied, the majority of tumors had a maximal tumor diameter ranging from 1 to 3 mm. In animals injected with 1×10^5 MLL/NIS cells, a large number of tumors had formed and coalesced, making accurate measurement of tumor diameters impossible (Fig. 3, bottom row).

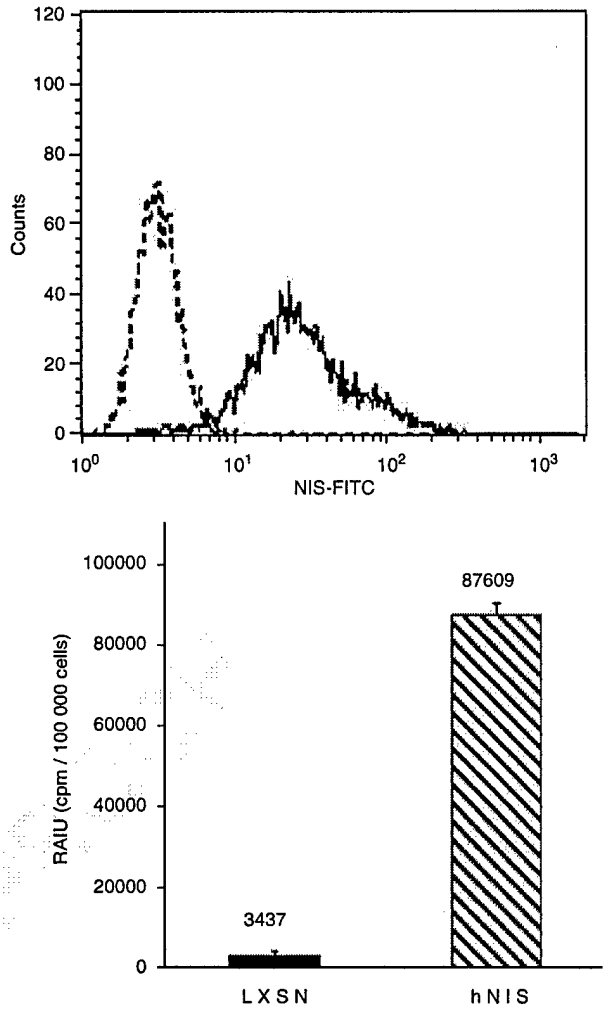

Figure 1 *In vitro* characterization of MLL/NIS cell line. Upper panel: Flow cytometry analysis showed that surface NIS expression was detectable in 85% of MLL/NIS cells. MLL/NIS cells were incubated with VJ2 α-NIS monoclonal antibody followed by FITC-labeled α-mouse (solid line) or with FITC-labeled α-mouse alone (dashed line). Lower panel: MLL/NIS cells showed a 25-fold increase in ^{125}I uptake, compared to vector-only cells (LXSN).

Multiple, distinct pulmonary tumor nodules can be detected with ^{99m}Tc SPECT

In animals not injected with tumor cells (Fig 3, top row), ^{99m}Tc uptake was only detectable in tissues that express endogenous NIS, such as the stomach (St), salivary gland (SG), and thyroid gland (Th). Following injection of 1×10^5 MLL/NIS cells (Fig 3, bottom row), the tumors had coalesced, and distinct lung nodules could not be identified by SPECT. In mice injected with 1×10^4 MLL/NIS cells (Fig 3, middle row), distinct lesions were detectable by SPECT. Multiple, discrete ^{99m}Tc-avid lesions are clearly visible in serial transverse images generated following image reconstruction (Fig 4). Post-mortem analysis of the lungs revealed the presence of 22

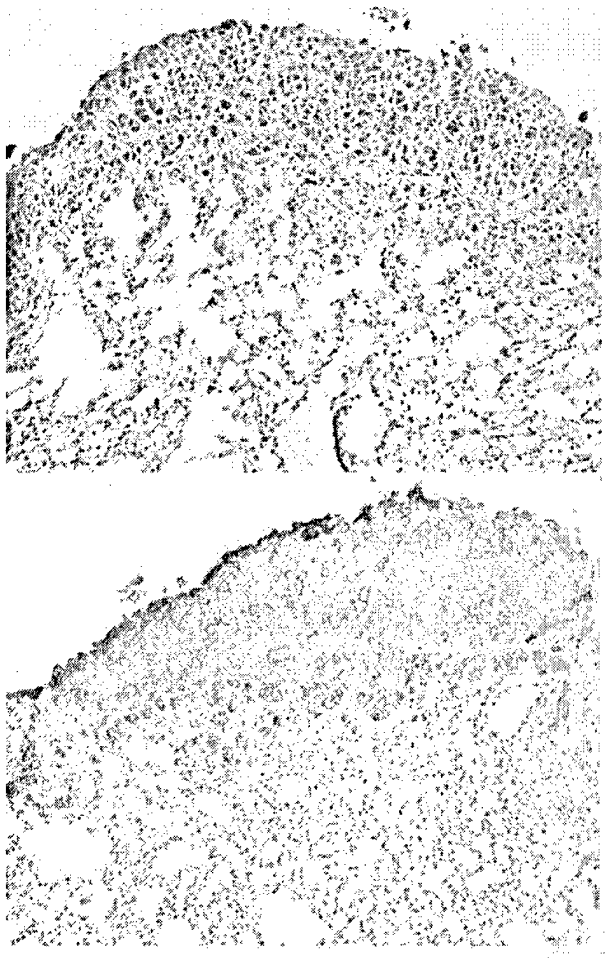

Figure 2 Immunohistochemical staining of NIS in vector-only MLL cells (upper panel) and in MLL/NIS cells (lower panel). Positive membrane staining was detected in MLL/NIS tumor cells, interspersed with nonstaining cells. Paraffin-embedded tissues were sectioned at 10 m thickness. Sections were incubated with polyclonal α-NIS antibody #331, detected with an α-rabbit 2^0 Ab conjugated to horseradish peroxidase, and counterstained with hematoxylin (×20).

surface tumors, compared to 14 areas of ^{99m}Tc uptake detected by SPECT (Fig. 3, middle row). Owing to the lack of reference points defining pulmonary anatomy in SPECT, it was not possible to precisely correlate ^{99m}Tc-vid lesions with tumor location post mortem.

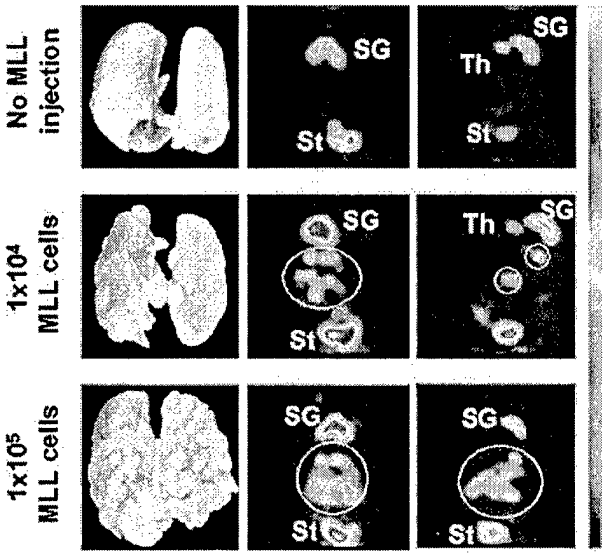

Figure 3 Injection of 1×10^4 MLL/NIS cells via tail vein results in distinct pulmonary tumor nodules that are detectable by SPECT imaging. The left column is gross pathology, the middle column is an anterior view of a reconstructed 3D image, and the right column is a sagittal view of a reconstructed 3D image. Image acquisition was performed 30 minutes after i.p. injection of 1 mCi of $Na^{99m}TcO_4$. In the animal not injected with tumor cells (top row), radionuclide uptake is only detectable in the stomach (St), salivary gland (SG), and thyroid (Th). In mice injected with MLL/NIS cells via tail vein (bottom two rows), examples of ^{99m}Tc-avid pulmonary lesions are circled. Note that separate tumor nodules are detectable in the animal imaged on DPI 18 with 1×10^4 MLL/NIS cells (middle row). By contrast, in the animal imaged on DPI 14 with 1×10^5 MLL/NIS cells (bottom row), lung tumors have coalesced, and distinct lung nodules cannot be identified.

Anatomic location of pulmonary MLL/NIS tumors can be defined using dual-isotope SPECT

In order to define the anatomic location of NIS-mediated radionuclide uptake detectable by SPECT, we performed simultaneous, dual-isotope imaging of MLL/NIS lung tumor nodules. Mice were given an i.p. injection of ^{125}I to image MLL/NIS tumors and a tail vein injection of macroaggregated albumin, labeled with ^{99m}Tc (^{99m}Tc-MAA), to image pulmonary perfusion. By using ^{99m}Tc-MAA to define pulmonary anatomy, we were able to determine the anatomic location of the ^{125}I-avid lesions.

Table 1 *In vivo* characterization of MLL/NIS tumor formation in the lungs of nude mice

Number of MLL cells injected	Mice (*n*)	Earliest date of detection by A-SPECT	Number of surface nodules	Surface nodule diameter (%)			
				<1 mm	1–2 mm	2–3 mm	>3 mm
2×10^3	2	DP120	37–72	12	49	35	5
1×10^4	4	DP117	8–36	21	44	26	8
1×10^5	11	DP114	>200	ND			

Nude mice were injected with different numbers of MLL/NIS cells via tail vein in a volume of 0.25 ml. SPECT studies were performed 30 minutes after i.p. injection of 1 mCi of $Na^{99m}TcO_4$, every 3–5 days postnjection (DPI). ND = not determined.

NPG.CGT.7700661

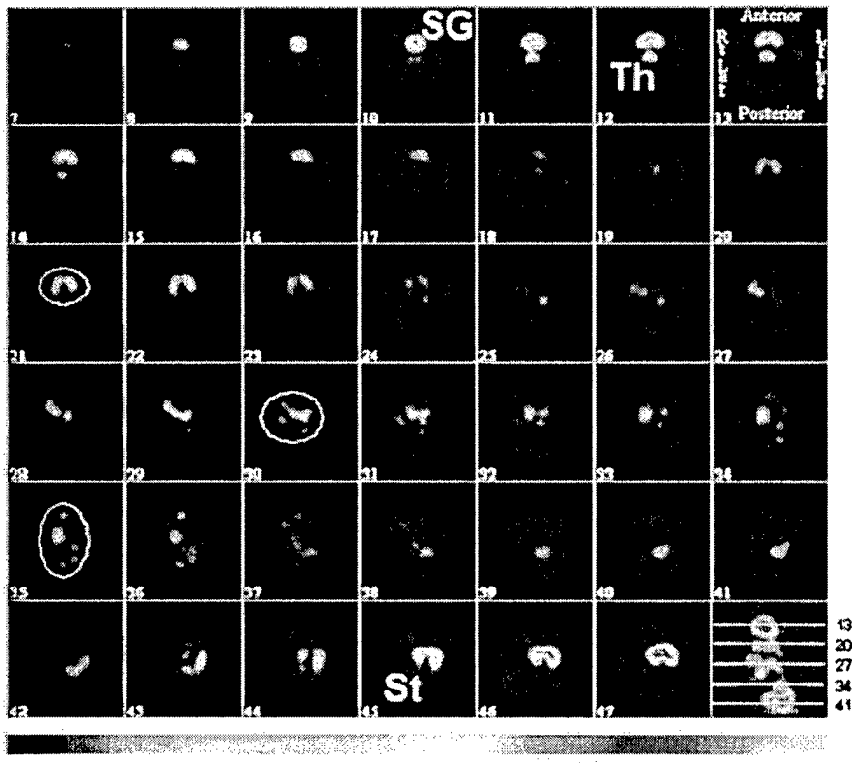

Figure 4 Serial transverse slices from a ^{99m}Tc SPECT study of a mouse bearing MLL/NIS pulmonary tumor nodules. Each slice is 0.59 mm in thickness, as calculated from the field of view. Image acquisition was performed 30 minutes after i.p. injection of 1 mCi of ^{99m}Tc, on DPI 18 with 1×10^4 MLL/NIS cells via tail vein. The relative locations of the individual slices are indicated in the reference frame (lower right corner). Examples of ^{99m}Tc-avid pulmonary lesions are circled. In addition, tissues expressing endogenous NIS, such as the stomach (St), salivary gland (SG), and thyroid (Th) are detected.

Post-mortem analysis of the lungs revealed the presence of eight surface tumors, three of which correlated to the location of the ^{125}I-avid lesions detected by SPECT (Fig 5). All three of the tumors detectable by SPECT had a maximal diameter of at least 3 mm (two were 3 mm in diameter and one was 4 mm). By contrast, the tumors not detected by SPECT had maximal diameters less than 3 mm (one was <1 mm, one was 2 mm, and the remaining three ranged between 1 and 2 mm). Thus, we concluded that a diameter of 3 mm was sufficient for tumor detection by SPECT with pinhole collimation.

Discussion

The utility of NIS to serve as an imaging reporter gene depends on several variables that have not yet been characterized. The minimum amount of NIS expression required for optimal detection *in vivo* and the minimal tumor size required for optimal detection must be determined and are likely interdependent. In addition, the sensitivity and quality of NIS imaging among various radionuclides and imaging modalities, such as planar scintigraphy, SPECT, and PET, should be compared. Finally, the utility of NIS as an imaging reporter gene will depend on the signal-to-noise ratio, which will differ based upon the tissue properties in which the tumor is located.

The minimal tumor size required for detection *in vivo* by nuclear imaging is affected by several variables, such as the level of NIS expression and the percentage of NIS-expressing cells in targeted tumors, as well as the radionuclide employed. Our studies employed a mixed population of NIS-expressing cells, which may have contributed to the inability to detect all tumor nodules visible at necropsy using SPECT. It has recently been demonstrated that NIS-negative cells grow more rapidly than NIS-positive cells in nude mice.[24] It would be of great interest to correlate the detectability of a given tumor with the percentage of NIS-expressing cells in our animal model. Further studies will be required to determine the degree to which the percentage of NIS-positive cells affects the minimal detectable tumor size. In addition, level of NIS expression will also affect the ability to detect NIS-expressing tumors. Our MLL/NIS cells express a relatively high level of NIS, displaying a 25-fold increase in radioiodide uptake *in vitro*. The use of a tumor model with inducible NIS expression should provide answers regarding the minimal expression level of NIS

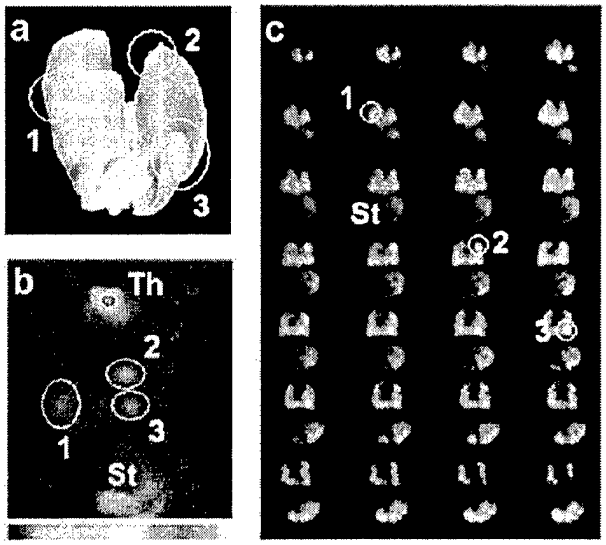

Figure 5 Dual-isotope SPECT study of a mouse bearing MLL/NIS lung tumor nodules. SPECT was performed on DPI 20 with 1×10^4 MLL/NIS cells via tail vein. **(a)** Gross pathology of the lungs removed after A-SPECT imaging. Three large tumors are visible on the surface of the lung (circled). **(b)** Anterior view of a reconstructed 3D image, acquired 2 hours after i.p. injection of 1 mCi of $Na^{125}I$. Three ^{125}I-avid lesions are visible, as are the thyroid gland (Th) and the stomach (St). **(c)** Serial frontal slices from a simultaneous SPECT study using ^{125}I and ^{99m}Tc-MAA. Each slice is 0.59 mm in thickness, as calculated from the field of view. In order to perform dual-isotope imaging simultaneously, 1 mCi of $Na^{125}I$ and 1 mCi of ^{99m}Tc-MAA were injected 2 hours (i.p.) and 30 minutes (tail vein) prior to image acquisition, respectively. Uptake of ^{125}I by the three tumor nodules and the stomach is shown in green. Pulmonary perfusion, as detected by ^{99m}Tc-MAA, is shown in red.

required for *in vivo* detection. A systematic evaluation of the level of NIS expression and the percentage and minimal number of NIS-expressing cells required for detection should provide insight into the limitations of using NIS as an imaging reporter gene.

Using ^{125}I SPECT, we were able to distinguish multiple, discrete lung tumors as small as 3 mm in diameter. It may be possible to detect tumors with smaller diameters using ^{99m}Tc SPECT, due to the higher energy and decreased tissue attenuation of ^{99m}Tc relative to ^{125}I. Although our results are not directly applicable to human studies (due to the inability to use pinhole collimation for whole lung field imaging and the weak gamma emission of ^{125}I), the ability to detect ^{125}I accumulation using SPECT in small animals is noteworthy. ^{125}I is commonly used in *ex vivo* molecular biology studies to label oligonucleotides, antibodies, ligands, and pharmaceuticals. These compounds can be iodinated relatively easily, and the long half-life ^{125}I (60 days) makes it favorable for longitudinal studies *in vivo*. Thus, ^{125}I SPECT could be a useful technique to determine the biologic half-life and biodistribution of a variety of iodinated compounds in preclinical small animal studies.

The feasibility of NIS as an imaging reporter gene has now been demonstrated using all three nuclear medicine imaging modalities: planar scintigraphy, SPECT, and PET. It will be interesting to compare the technical limitations and image quality of these modalities in detecting NIS-mediated radionuclide accumulation. One important capability of SPECT that differentiates it from PET is dual-isotope imaging. Dual-isotope studies are a powerful tool for investigating multiple targets simultaneously using isotopes that emit photons of different energies. In contrast, PET scanners are restricted to detection of radiopharmaceuticals emitting 511 keV.[22] In our SPECT studies, we used ^{125}I to image MLL/NIS tumors and ^{99m}Tc-MAA to define pulmonary anatomy, allowing us to define the anatomic location of ^{125}I-avid tumors. These results demonstrate the potential use of SPECT to simultaneously analyze exogenous NIS expression with other physiologic parameters.

Both PET and SPECT studies are superior to planar scintigraphy because they permit 3D image reconstruction. In contrast, planar scintigraphy results in the loss of geometry due to compression into two dimensions and loss of sensitivity due to signal per volume averaging. The advantage of PET lies in its ability to quantify a wide variety of biochemical processes with high sensitivity.[25] The usefulness of PET in preclinical, small animal studies may be restricted, however, by the requirement for a local cyclotron, and the cost and short half-lives of the radionuclides generated. The use of SPECT to detect exogenous NIS has many potential advantages over PET, including the ability to detect readily available radionuclides, such as ^{131}I, ^{123}I, ^{125}I, and ^{99m}Tc. While it is not yet clear whether PET or SPECT will provide better resolution in small animal imaging, the ease of use and lower cost of SPECT make it an attractive technique for imaging NIS function.

The ability to localize NIS-mediated radionuclide uptake anatomically will be enhanced by the addition of X-ray micro computed tomography (micro-CT).[26] CT will allow coregistration of CT-SPECT images and the selection of regions of interest on the anatomic images from the CT. These regions can then be used to extract radioisotope counts from the SPECT raw data and quantitatively analyze NIS-mediated uptake. In addition, the presence of CT will allow SPECT images to be corrected for scatter and tissue attenuation following reconstruction. The ability to accurately quantify the amount of radionuclide accumulation will be essential for the use of NIS as a surrogate marker for therapeutic gene expression in preclinical animal models.

In this study, we demonstrate that multiple, discrete NIS-expressing pulmonary tumors can be detected *in vivo* using ^{99m}Tc and ^{125}I SPECT with pinhole collimation. The finding that a higher number of injected cells correlated with an earlier date of tumor detection indicates that a minimal number of NIS-expressing cells and/or target tissue size are required for *in vivo* detection. Finally, the combination of dual-isotope SPECT and post-mortem analysis shows that NIS-expressing pulmonary tumors as small as 3 mm in diameter can be detected by ^{125}I SPECT.

Acknowledgments

We thank our colleagues in the Division of Nuclear Medicine, including Ms Bonnie Williams, Mr Cowan Edwards, and Mr Aaron Haynam for the preparation of radionuclides. In addition, we also thank Dr W Yang for his assistance with tail vein injections. This work was supported by DOD Prostate Cancer Research Program DAMD 17-02-0119 (to SMJ) and by the NIH T32 DE14320 from the National Institute of Dental and Craniofacial Research (to DKM).

References

1. Jhiang SM. Regulation of sodium/iodide symporter. *Rev Endocr Metab Disord.* 2000;1:205–215.
2. Castro MR, Bergert ER, Beito TG, et al. Monoclonal antibodies against the human sodium iodide symporter: utility for immunocytochemistry of thyroid cancer. *J Endocrinol.* 1999;163:495–504.
3. Dai G, Levy O, Carrasco N. Cloning and characterization of the thyroid iodide transporter. *Nature.* 1996;379:458–460.
4. Smanik PA, Liu Q, Furminger TL, et al. Cloning of the human sodium iodide symporter. *Biochem Biophys Res Commun.* 1996;226:339–345.
5. Kotani T, Ogata Y, Yamamoto I, et al. Characterization of gastric Na+/I- symporter of the rat. *Clin Immunol Immunopathol.* 1998;89:271–278.
6. Vayre L, Sabourin JC, Caillou B, Ducreux M, Schlumberger M, Bidart JM. Immunohistochemical analysis of Na+/I-symporter distribution in human extra-thyroidal tissues. *Eur J Endocrinol.* 1999;141:382–386.
7. Jhiang SM, Cho JY, Ryu KY, et al. An immunohistochemical study of Na+/I- symporter in human thyroid tissues and salivary gland tissues. *Endocrinology.* 1998;139:4416–4419.
8. Spitzweg C, Joba W, Schriever K, Goellner JR, Morris JC, Heufelder AE. Analysis of human sodium iodide symporter immunoreactivity in human exocrine glands. *J Clin Endocrinol Metab.* 1999;84:4178–4184.
9. Josefsson M, Grunditz T, Ohlsson T, Ekblad E. Sodium/iodide-symporter: distribution in different mammals and role in entero-thyroid circulation of iodide. *Acta Physiol Scand.* 2002;175:129–137.
10. Tazebay UH, Wapnir IL, Levy O, et al. The mammary gland iodide transporter is expressed during lactation and in breast cancer. *Nat Med.* 2000;6:871–878.
11. Cho JY, Leveille R, Kao R, et al. Hormonal regulation of radioiodide uptake activity and Na+/I- symporter expression in mammary glands. *J Clin Endocrinol Metab.* 2000;85:2936–2943.
12. Shen DH, Kloos RT, Mazzaferri EL, Jhiang SM. Sodium iodide symporter in health and disease. *Thyroid.* 2001;11:415–425.
13. Shimura H, Haraguchi K, Miyazaki A, Endo T, Onaya T. Iodide uptake and experimental 131I therapy in transplanted undifferentiated thyroid cancer cells expressing the Na+/I- symporter gene. *Endocrinology.* 1997;138:4493–4496.
14. Mandell RB, Mandell LZ, Link Jr CJ. Radioisotope concentrator gene therapy using the sodium/iodide symporter gene. *Cancer Res.* 1999;59:661–668.
15. Spitzweg C, O'Connor MK, Bergert ER, Tindall DJ, Young CY, Morris JC. Treatment of prostate cancer by radioiodine therapy after tissue-specific expression of the sodium iodide symporter. *Cancer Res.* 2000;60:6526–6530.
16. Haberkorn U, Henze M, Altmann A, et al. Transfer of the human NaI symporter gene enhances iodide uptake in hepatoma cells. *J Nucl Med.* 2001;42:317–325.
17. Boland A, Ricard M, Opolon P, et al. Adenovirus-mediated transfer of the thyroid sodium/iodide symporter gene into tumors for a targeted radiotherapy. *Cancer Res.* 2000;60:3484–3492.
18. La Perle KM, Shen D, Buckwalter TL, et al. *In vivo* expression and function of the sodium iodide symporter following gene transfer in the MATLyLu rat model of metastatic prostate cancer. *Prostate.* 2002;50:170–178.
19. Cho JY, Shen DH, Yang W, et al. *In vivo* imaging and radioiodine therapy following sodium iodide symporter gene transfer in animal model of intracerebral gliomas. *Gene Ther.* 2002;9:1139–1145.
20. Dingli D, Diaz RM, Bergert ER, O'Connor MK, Morris JC, Russell SJ. Genetically targeted radiotherapy for multiple myeloma. *Blood.* 2003;102:489–496.
21. Groot-Wassink T, Aboagye EO, Glaser M, Lemoine NR, Vassaux G. Adenovirus biodistribution and noninvasive imaging of gene expression *in vivo* by positron emission tomography using human sodium/iodide symporter as reporter gene. *Hum Gene Ther.* 2002;13:1723–1735.
22. King MA, Pretorius PH, Farncombe T, Beekman FJ. Introduction to the physics of molecular imaging with radioactive tracers in small animals. *J Cell Biochem Suppl.* 2002;39:221–230.
23. Pohlenz J, Duprez L, Weiss RE, Vassart G, Refetoff S, Costagliola S. Failure of membrane targeting causes the functional defect of two mutant sodium iodide symporters. *J Clin Endocrinol Metab.* 2000;85:2366–2369.
24. La Perle KM, Blomme EA, Capen CC, Jhiang SM. Effect of exogenous human sodium iodide symporter expression on growth of MATLyLu cells. *Thyroid.* 2003;13:133–140.
25. Myers R, Hume S. Small animal PET. *Eur Neuropsychopharmacol.* 2002;12:545–555.
26. Ritman EL. Molecular imaging in small animals-roles for micro-CT. *J Cell Biochem Suppl.* 2002;39:116–124.